Diurnal variations of $BrONO_2$ observed by MIPAS-B at mid-latitudes and in the Arctic

Gerald Wetzel[1], Hermann Oelhaf[1], Michael Höpfner[1], Felix Friedl-Vallon[1], Andreas Ebersoldt[2], Thomas Gulde[1], Sebastian Kazarski[1], Oliver Kirner[3], Anne Kleinert[1], Guido Maucher[1], Hans Nordmeyer[1], Johannes Orphal[1], Roland Ruhnke[1], and Björn-Martin Sinnhuber[1]

[1]Karlsruhe Institute of Technology, Institute of Meteorology and Climate Research, Karlsruhe, Germany

[2]Karlsruhe Institute of Technology, Institute for Data Processing and Electronics, Karlsruhe, Germany

[3]Karlsruhe Institute of Technology, Steinbuch Centre for Computing, Karlsruhe, Germany

Correspondence to: Gerald Wetzel (gerald.wetzel@kit.edu)

Abstract

The first stratospheric measurements of the diurnal variation of the inorganic bromine (Br_y) reservoir species $BrONO_2$ around sunrise and sunset are reported. Arctic flights of the balloon-borne Michelson Interferometer for Passive Atmospheric Sounding (MIPAS-B) were carried out from Kiruna (68°N, Sweden) in January 2010 and March 2011 inside the stratospheric polar vortices where diurnal variations of $BrONO_2$ around sunrise have been observed. High nighttime $BrONO_2$ volume mixing ratios of up to 21 parts per trillion by volume (pptv) were detected in the late winter 2011 in the absence of polar stratospheric clouds (PSCs). In contrast, the amount of measured $BrONO_2$ was significantly lower in January 2010 due to low available NO_2 amounts (for the build-up of $BrONO_2$), heterogeneous destruction of $BrONO_2$ on PSC particles, and the gas-phase interaction of BrO (the source to form $BrONO_2$) with ClO. A further balloon flight took place at mid-latitudes from Timmins (49°N, Canada) in September 2014. Mean $BrONO_2$ mixing ratios of 22 pptv were observed after sunset in the altitude region between 21 and 29 km. Measurements are compared and discussed with the results of a multi-year simulation performed with the chemistry climate model ECHAM5/MESSy Atmospheric Chemistry (EMAC). The calculated temporal variation of $BrONO_2$ is in principal agreement with the balloon-borne observations. Using the nighttime simulated ratio between $BrONO_2$ and Br_y, the amount of Br_y observed by MIPAS-B was estimated to about 21-25 pptv in the lower stratosphere.

1 Introduction

Chlorine and bromine species play a dominant role in the contribution to ongoing stratospheric ozone depletion since the amount of equivalent effective stratospheric chlorine (chlorine and bromine) is predicted to return to 1980 values by 2050 at mid-latitudes (Newman et al., 2007; Stolarski et al., 2010). $BrONO_2$ is, besides BrO, the most abundant inorganic bromine (Br_y) compound in the stratosphere (see e.g. Brasseur and Solomon, 2005; Sinnhuber et al., 2009; Sinnhuber and Meul, 2015). $BrONO_2$ is formed via the reaction with BrO and NO_2:

$$BrO + NO_2 + M \rightarrow BrONO_2 + M. \quad (R1)$$

During day, $BrONO_2$ is photolyzed with different possible channels

$$BrONO_2 + h\nu \rightarrow Br + NO_3 \quad (R2a)$$

$$\rightarrow BrO + NO_2 \quad (R2b)$$

with a higher quantum yield of (R2a) compared to (R2b). $BrONO_2$ can also be destroyed via the reaction with atomic oxygen:

$$BrONO_2 + O(^3P) \rightarrow BrO + NO_3. \quad (R3)$$

(R1) to (R3) exhibit the close connection between BrO and $BrONO_2$ leading to an opposite diurnal variation of these species. Gas-phase $BrONO_2$ can also be converted to gas-phase HOBr and BrCl on sulphate aerosols and polar stratospheric cloud (PSC) particles where H_2O, HCl, and HNO_3 are in liquid (l) or solid phase (s):

$$BrONO_2 + H_2O\ (l, s) \rightarrow HOBr + HNO_3\ (l, s) \quad (R4)$$

$$BrONO_2 + HCl\ (l, s) \rightarrow BrCl + HNO_3\ (l, s). \quad (R5)$$

An interaction between the chlorine and bromine family (particularly important at high latitudes in winter under conditions of elevated ClO) is the gas-phase production of BrCl via:

$$ClO + BrO \rightarrow BrCl + O_2. \quad (R6)$$

Stratospheric $BrONO_2$ was detected for the first time by the Michelson Interferometer for Passive Atmospheric Sounding (MIPAS) aboard the Envisat satellite (Höpfner et al., 2009). Strong day/night variations were observed with much lower concentrations during day compared to nighttime. A maximum amount of 20-25 pptv (parts per trillion by volume) was inferred from MIPAS spectra recorded during the night.

Flights of the balloon version of the MIPAS instrument (MIPAS-B) investigated in this work were carried out from Kiruna (68°N, Sweden) on 24 January 2010 and 31 March 2011 as well as from Timmins (49°N, Canada), on 7/8 September 2014. For the first time, diurnal variations of $BrONO_2$ around sunrise (Kiruna flights) and sunset (Timmins flight) were measured by MIPAS-B with high temporal resolution. A description of the MIPAS-B instrument, data analysis and chemical modelling is given in Sect. 2. A discussion of observed $BrONO_2$ volume mixing ratio (VMR) vertical profiles follows in Sect. 3 together with a comparison of the measured data to simulations of the chemistry climate model ECHAM5/MESSy Atmospheric Chemistry (EMAC) to check the current understanding of stratospheric bromine chemistry and to estimate the amount of lower stratospheric Br_y.

2 MIPAS-B instrument, data analysis and modelling

In the following sections, we give an overview of the MIPAS-B instrument and the balloon flights together with the corresponding data analysis and a description of chemical modelling performed for this study.

2.1 MIPAS-B instrument and balloon flights

The balloon-borne cryogenic Fourier Transform limb emission spectrometer operates in the mid-infrared spectral region between about 4 and 14 µm. The maximum optical path difference of 14.5 cm of the beam in the interferometer correlates with 0.0345 cm^{-1} spectral resolution. This corresponds to about 0.07 cm^{-1} after apodization with the Norton and Beer (1976) "strong" function and allows the separation of individual spectral lines from continuum-like emissions. Noise equivalent spectral radiance (NESR) values for a single calibrated spectrum are typically within $1x10^{-9}$ and $7x10^{-9}$ $W(cm^2\ sr\ cm^{-1})^{-1}$. A reduction of spectral noise by a factor of $n^{-0.5}$ is obtained by recording and averaging of n spectra ($n \leq 16$) per single elevation scan. Besides a high radiometric accuracy of typically 1%, the pointing system allows a knowledge of the tangent altitude of better than 50 m at the 1-σ confidence limit. An overview of instrument characterization in terms of the instrumental line shape, field of view, NESR, line of sight of the instrument, detector non-linearity (Kleinert, 2006) and the error assessment of the calibrated spectra is given by Friedl-Vallon et al. (2004).

In this study, we report $BrONO_2$ results from three MIPAS-B flights. Details are shown in Table 1. The first flight took place on 24 January 2010 from Kiruna over northern Scandinavia inside

the Arctic vortex at the beginning of a major stratospheric warming (Wetzel et al., 2012). The second one was carried out from the same location on 31 March 2011 inside a still persistent late-winter Arctic vortex (Wetzel et al., 2015). The third one was performed at mid-latitudes from Timmins (Ontario, Canada) on 7 to 8 September 2014. For this mid-latitude flight, we show retrieval results from spectra observed around sunset. For the Arctic flights, MIPAS-B measurements were performed from night into day. All flights have in common that fast sequences of spectra were recorded in short time steps of about 10 min to enable the retrieval of photochemically active species, which change quickly their concentration around sunrise and sunset. The line of sight of the instrument was aligned perpendicular to the azimuth direction of the sun to allow for a symmetric illumination of the sounded air mass before and beyond the tangent point. The analysis of the recorded spectra is described in the following section.

2.2 Data analysis

Radiance calculations were carried out with the Karlsruhe Optimized and Precise Radiative transfer Algorithm (KOPRA; Stiller et al., 2002). Spectroscopic parameters for the calculation of emission spectra were taken from the high-resolution transmission molecular absorption database (HITRAN; Rothman et al., 2009) and a MIPAS dedicated line list (Raspollini et al., 2013). Spectral features of the molecule $BrONO_2$ were calculated using new pressure-temperature dependent absorption cross sections measured by Wagner and Birk (2016) with a 2% intensity accuracy. KOPRA also provides derivatives of the radiance spectrum with respect to atmospheric state and instrument parameters (Jacobians) which are used by the retrieval procedure KOPRAFIT (Höpfner et al., 2002). The vertical distance of tangent altitudes ranges between 1 and 1.5 km. Thus, the retrieval grid was set to 1 km up to the balloon float (observer) altitude. Above this level, the vertical spacing increases gradually up to 10 km at the top altitude of 100 km. Considering the smoothing of the vertical part of the instrumental field of view, the retrieval grid is somewhat finer than the achievable vertical resolution of the measurement for most parts of the altitude region covered (especially above the observer altitude). To avoid retrieval instabilities caused by this oversampling, a Tikhonov-Phillips regularization approach (Phillips, 1962; Tikhonov, 1963) was applied using a constraint with respect to a first derivative of the a priori profile $\boldsymbol{x}_\mathrm{a}$ of the target species:

$$\boldsymbol{x}_{i+1} = \boldsymbol{x}_i + [\mathbf{K}_i^T \mathbf{S}_\mathrm{y}^{-1} \mathbf{K}_i + \mathbf{R}]^{-1} [\mathbf{K}_i^T \mathbf{S}_\mathrm{y}^{-1} (\boldsymbol{y}_\mathrm{meas} - \boldsymbol{y}(\boldsymbol{x}_i)) - \mathbf{R}(\boldsymbol{x}_i - \boldsymbol{x}_\mathrm{a})], \quad (1)$$

where $\boldsymbol{x}_{i+1}$ is the vector of the state parameters $\boldsymbol{x}_i$ for iteration i+1; $\boldsymbol{y}_{meas}$ is the measured radiance vector and $\boldsymbol{y}(\boldsymbol{x}_i)$ the calculated radiance using state parameters of iteration i; $\mathbf{K}$ is the Jacobian matrix with partial derivatives $\partial \boldsymbol{y}(\boldsymbol{x}_i)/\partial \boldsymbol{x}_i$ while $\mathbf{S}_y^{-1}$ is the inverse noise measurement covariance matrix and $\mathbf{R}$ a regularization matrix composed of the first derivative operator and a regularization strength parameter.

The $BrONO_2$ retrieval calculations were performed in the range of the ν_3 band centred at 803.37 cm^{-1}. Figure 1 shows spectral contributions of relevant species in the $BrONO_2$ microwindow from 801 to 820 cm^{-1} that has been found best appropriate to derive the $BrONO_2$ amount from MIPAS-B spectra. Besides the target molecule $BrONO_2$, all main interfering species H_2O, CO_2, O_3, NO_2, HNO_3, COF_2, HCFC-22 ($CHClF_2$), CCl_4, CFC-113 ($C_2Cl_3F_3$), $ClONO_2$, HO_2NO_2, and PAN (peroxyacetyl nitrate) were fitted simultaneously together with temperature, instrumental (radiometric) offset and wavenumber shift. The molecule HO_2NO_2 shows a similar spectral band shape like the target species $BrONO_2$. Since the HO_2NO_2 absorption cross sections (included in HITRAN) measured by May and Friedl (1993) are derived at only one temperature (220 K) a second set of cross sections derived by Friedl et al. (1994) at room temperature (298 K) was used to allow a two-point interpolation of the cross section intensity to the current atmospheric temperature.

Vertical profiles of minor contributing species were either adjusted in appropriate microwindows prior to the $BrONO_2$ retrieval or taken from a climatological atmosphere (Remedios et al., 2007), updated with surface concentration data from NOAA ESRL GMD (National Oceanic and Atmospheric Administration, Earth System Research Laboratory, Global Monitoring Division; Montzka et al., 1999). An example of a best fit of a measured MIPAS-B spectrum zoomed around the Q-branch region of the $BrONO_2$ ν_3 band for a tangent altitude near 20 km is shown in Figure 2. The spectrum was recorded during night. If the fit is performed in absence of $BrONO_2$ in the model atmosphere, a systematic residual is remaining around the centre of the $BrONO_2$ Q-branch at 803.37 cm^{-1} (blue solid line in Figure 2). If the molecule $BrONO_2$ is taken into account by the radiative transfer calculation, the systematic residual around the Q-branch disappears demonstrating the existence of $BrONO_2$ in the stratosphere. Another example for a best fit in the same altitude region but for a MIPAS-B spectrum recorded during day is illustrated in Figure 3. Here, we recognize that for a daytime situation the effect whether the species $BrONO_2$ is included in the radiative transfer calculations or not, is clearly smaller compared to the nighttime case (cf. Figure 2) such that we expect lower

stratospheric $BrONO_2$ VMRs during day and higher values at night. This is confirmed by the retrieved vertical profiles of $BrONO_2$ illustrated in Figures 4 and 5 together with the error budget and altitude resolution. The dominant part of the total error in the $BrONO_2$ retrieval is spectral (random) noise resulting in a $BrONO_2$ VMR error of about 2 to 4 pptv (10-25%) in the altitude region of the VMR maximum. An important systematic error source are uncertainties of disturbing gases overlapping the $BrONO_2$ ν_3 band. This influence was estimated using uncertainties in line intensity and half-width as given by Flaud et al. (2003) and HITRAN (Rothman et al., 2009) and results into a $BrONO_2$ error of up to 2 pptv (10-20%) in the altitude region of the $BrONO_2$ VMR maximum. Retrieval simulations of the major interfering species O_3, CO_2, and H_2O have revealed an influence (line half-width and intensity uncertainties) within 10% on the $BrONO_2$ amount (Höpfner et al., 2009). The species $ClONO_2$, followed by HO_2NO_2 have large contributions to the limb emission spectra (see Figure 1). Temperature and pressure dependent $ClONO_2$ absorption cross sections were measured by Wagner and Birk (2003) with high accuracy. Systematic errors in the $BrONO_2$ VMR due to $ClONO_2$ spectroscopy are expected to be within 10% (Wagner and Birk, 2016). As mentioned above, a temperature dependence of HO_2NO_2 absorption cross sections was included to improve spectroscopy of this interfering species. Further systematic error sources like radiometric gain, line of sight, and the spectroscopy of the target molecule $BrONO_2$ itself are of minor importance for the total error budget of the $BrONO_2$ retrieval (see Figures 4 and 5). The altitude resolution of the retrieved $BrONO_2$ profiles was calculated from the full width at half maximum (FWHM) of the rows of the averaging kernel matrix. It amounts to between about 4 and 6 km (~ 4-5 degrees of freedom) over a wide range in the stratosphere (see right column of Figures 4 and 5).

2.3 Model calculations

Measured MIPAS-B data are compared to a multi-year simulation of the chemistry climate model EMAC that includes sub-models describing tropospheric and middle atmosphere processes (Jöckel et al., 2010). The core atmospheric model is the 5th generation European Centre Hamburg general circulation model (ECHAM5; Roeckner et al., 2006) which is linked to the sub-models via the interface Modular Earth Submodel System (MESSy). For the present study we applied EMAC (ECHAM5 version 5.3.02, MESSy version 2.52) in the T42L90MA-resolution, i.e., with a spherical truncation of T42 (corresponding to a Gaussian grid of approximately 2.8 by 2.8 degrees in latitude and longitude) and 90 vertical hybrid pressure levels from the ground up to 0.01 hPa (approx. 80 km). The calculation of gas-phase chemistry

is realized by the submodel MECCA (Sander et al., 2005). The submodel MSBM (Kirner et al., 2011) simulates polar stratospheric clouds and calculates heterogeneous reaction rates.

A Newtonian relaxation technique of the surface pressure and the prognostic variables temperature, vorticity, and divergence above the boundary layer and below 1 hPa towards the ECMWF reanalysis ERA-Interim (Dee et al., 2011) has been applied to simulate realistic synoptic conditions (van Aalst, 2005). The simulation includes a comprehensive chemistry setup from the troposphere to the lower mesosphere with more than 100 species involved in gas phase-, photolysis-, and heterogeneous reactions on liquid sulphate aerosols, nitric acid trihydrate (NAT) and ice particles. Rate constants of gas-phase reactions originate from Atkinson et al. (2007) and the Jet Propulsion Laboratory (JPL) compilation (Sander et al., 2011). Photochemical reactions of short-lived bromine-containing organic compounds CH_3Br, $CHBr_3$, CH_2Br_2, CH_2ClBr, $CHClBr_2$, and $CHCl_2Br$ are integrated into the model setup (Jöckel et al., 2016). Surface emissions of these species are taken from scenario 5 of Warwick et al. (2006). During the time period with MIPAS-B balloon flights the model output data were saved every 10 minutes. The temporally closest model output to the MIPAS-B measurements was interpolated in space to the observed geolocations.

3 Results and discussion

In this section, vertical profiles retrieved from MIPAS-B limb emission spectra measured before and after sunrise (Arctic flights) and sunset (mid-latitude flight) are shown. The measured data have been temporally smoothed with a 3-point adjacent averaging routine to attenuate noisy structures. These data were compared to EMAC simulations. To permit a more realistic comparison with respect to different altitude resolutions in the measurement and the simulation, EMAC vertical profiles were additionally smoothed with the averaging kernel matrix and the a priori profile of MIPAS-B. A smoothed EMAC profile $\boldsymbol{x}_s$ is calculated following the method described in Rodgers (2000):

$$\boldsymbol{x}_s = \boldsymbol{x}_a + \mathbf{A}(\boldsymbol{x} - \boldsymbol{x}_a^*), \quad (2)$$

where $\boldsymbol{x}_a$ is the a priori profile of MIPAS-B, $\boldsymbol{x}_a^*$ the a priori profile interpolated to the altitude grid of the EMAC profile $\boldsymbol{x}$, and $\mathbf{A}$ is the averaging kernel matrix of MIPAS-B.

3.1 Arctic measurements

The temporal evolution of $BrONO_2$ measured during the balloon flight from Kiruna on 31 March 2011 inside the late winter stratospheric polar vortex is shown in Figure 6. No PSCs were present during the time of the MIPAS-B measurement (Wetzel et al., 2015). A nighttime maximum of $BrONO_2$ around 25 km with values of more than 20 pptv is clearly visible. After sunrise, the amount of $BrONO_2$ decreases to maximum values of about 14 pptv around 22 km. This downward displacement of the VMR maximum in terms of altitude can be explained by photolysis. Towards higher altitudes, the decomposition of $BrONO_2$ according to (R2a), (R2b), and (R3) is increasingly faster than the $BrONO_2$ build-up via (R1). The overall structure (including the VMR altitude displacement) of the simulated temporal evolution of $BrONO_2$ is similar to the measured one and is shown in Figure 7 together with the temporal development of the directly linked molecule BrO (Figure 8). Maximum nighttime $BrONO_2$ values in EMAC are comparable to the measured amounts. However, above the nocturnal VMR maximum, EMAC calculates higher $BrONO_2$ concentrations compared to the balloon observation (see Figure 9). Furthermore, the daytime photochemical destruction of $BrONO_2$ is slightly faster in the model yielding several pptv lower daytime $BrONO_2$ VMRs in the model compared to MIPAS-B. The EMAC simulation smoothed with the averaging kernel matrix of MIPAS-B according to Eq. (2) is displayed in Figure 10. A main difference to the unsmoothed case shown in Figure 7 is the reduction of the nighttime $BrONO_2$ VMR at altitudes above the maximum that yields to a better agreement with measured $BrONO_2$ (see Figure 11).

Another Arctic balloon flight was performed from Kiruna on 24 January 2010 inside a cold polar vortex under mid-winter weak illumination conditions. As a consequence of low stratospheric temperatures in this winter, widespread PSCs were present in an altitude region between about 18 and 24 km at the time of the MIPAS-B observation (Wetzel et al., 2012). The observed $BrONO_2$ as seen from night until noon is shown in Figure 12. Nighttime $BrONO_2$ mixing ratios are clearly lower compared to the previously discussed situation in late March 2011. This is also reflected in the EMAC simulation (Figure 13) although there are some differences visible with regard to the observation (see Figure 14). During the long polar night the amount of available NO_2 (Wetzel et al. 2012) to produce $BrONO_2$ via (R1) is significantly reduced due to the conversion of NO_2 into its reservoir species (mainly HNO_3). In this period of darkness, nearly all $BrONO_2$ below 25 km (PSC region) is converted to BrCl via heterogeneous chemistry according to (R5) and gas-phase conversion of BrO to BrCl via (R6).

Here, more than 90 % of Br_y are in the form of BrCl in the model simulation during night. Above this altitude region, $BrONO_2$ and BrCl together are the dominant species of the nocturnal Br_y budget in the EMAC run. During day, photolyzation of both species ($BrONO_2$ and BrCl) leads to an increase of BrO such that this species then dominates the Br_y budget. If we smooth the EMAC $BrONO_2$ data with the averaging kernel matrix of MIPAS-B, we see a better agreement with MIPAS-B in the structure of the temporal evolution of the $BrONO_2$ amount (see Figures 15 and 16). The effect of the smoothing appears to be stronger compared to the case in March 2011 since low temperatures together with low amounts of $BrONO_2$ in January 2010 entailed to perform the retrieval with a factor of 2 coarser altitude resolution compared to a standard $BrONO_2$ retrieval setup as depicted in Figures 4 and 5.

3.2 Mid-latitude measurements

MIPAS-B spectra have been recorded from day until night over Ontario (Canada) during a balloon flight launched from Timmins on 7 September 2014. The temporal evolution of measured $BrONO_2$ is depicted in Figure 17. A significant increase of $BrONO_2$ starting shortly before sunset is visible. This is caused by the weakened illumination at SZAs near 90° that enables the build-up of $BrONO_2$ from daytime BrO via (R1). Nighttime $BrONO_2$ mixing ratios of more than 24 pptv are seen by MIPAS-B around 28 km altitude. The corresponding EMAC model simulation is displayed in Figure 18. The principal shape of the increase of $BrONO_2$ VMR is reproduced by the model run although absolute values in the altitude region of the VMR maximum are somewhat lower in the simulation compared to the measurement (see Figure 19). A sensitivity study based on measured BrO slant column densities performed by Kreycy et al. (2013) points to a possible stronger $BrONO_2$ photolysis rate and a lower reaction rate of the $BrONO_2$ build-up from BrO and NO_2 with respect to the JPL recommendation (Sander et al., 2011). However, own sensitivity studies with a 1-D photochemical stacked box model (Sinnhuber et al., 2005) have shown that using the Kreycy et al. (2013) recommendation leads to lower $BrONO_2$ values during day towards higher BrO amounts and thus further degrades the agreement between model simulations and our MIPAS-B measurements. During night, the simulated $BrONO_2$ VMR does not change significantly (< 0.1 pptv below 30 km). However, the Kreycy et al. (2013) study refers to Arctic September conditions and the outcome is therefore not directly comparable to the mid-latitude observations shown here.

Differences in absolute $BrONO_2$ amounts between EMAC and MIPAS-B are at least partly connected with the fact that EMAC NO_2 values are up to 20 % lower than the observed NO_2 in

the altitude region of the $BrONO_2$ VMR maximum. In the afternoon, the simulation already shows a weak temporal increase in $BrONO_2$ that is not seen by MIPAS-B. However, during the time of strongest increase (18:30-19:20 LST) differences between EMAC and MIPAS-B are small. (see Figure 19). Nighttime maximum $BrONO_2$ values in EMAC reach about 22 pptv and are located in the same altitude region as seen in the observation. Smoothing the EMAC data with the averaging kernel matrix of MIPAS-B yields to a better agreement with the structure of the observational data at altitudes below about 18 km (see Figures 20 and 21).

3.3 Estimation of inorganic bromine

As already discussed in Sect. 1, $BrONO_2$ is a dominant species of lower stratospheric inorganic bromine. Simulations with EMAC show that more than 90% of nocturnal Br_y is in the form of $BrONO_2$ between 21 and 29 km during the time of the MIPAS-B flight in September 2014. For comparison, the species BrO (not measurable by MIPAS-B) contributes not more than 80% to total Br_y during daytime in the altitude region of the MIPAS-B measurement). Furthermore, the concentration of BrO is gradually changing during day while the amount of $BrONO_2$ is rather constant during nighttime. Hence, $BrONO_2$ is best suited to estimate the amount of "measured" inorganic bromine [Br_y(meas)] from measured nighttime [$BrONO_2$(meas)] using the calculated [$BrONO_2$(mod)]/[Br_y(mod)] ratio from EMAC in the following form:

$$[\mathrm{Br_y\,(meas)}] = \frac{[\mathrm{BrONO_2\,(meas)}][\mathrm{Br_y\,(mod)}]}{[\mathrm{BrONO_2\,(mod)}]}. \qquad (3)$$

We now apply Eq. (3) for the MIPAS-B mid-latitude flight in September 2014 for a nighttime (SZA $\geq 99°$) ratio [$BrONO_2$(mod)]/[Br_y(mod)] ≥ 0.9 corresponding to an altitude region between 21 and 29 km. We then calculate [Br_y(meas)] (including the total [$BrONO_2$(meas)] error) to 23.6 ± 1.9 pptv. The given error bar represents the 1-σ total error originating from measured $BrONO_2$.

In the case of the Arctic flight in March 2011, the portion of $BrONO_2$ of total Br_y is slightly smaller compared to the mid-latitude situation. Applying Eq. (3) in an altitude region between 23 and 29 km, corresponding to a nighttime (SZA $\geq 96°$) ratio [$BrONO_2$(mod)]/[Br_y(mod)] ≥ 0.8, we calculate [Br_y(meas)] to 22.3 ± 2.2 pptv. An estimation of total Br_y from the MIPAS-B data obtained during the Arctic flight in January 2010 is not reasonable since measured $BrONO_2$ values are very low during this time of the winter.

Our estimated Br_y values can be compared to observations of stratospheric Br_y calculated with photochemical modelling using balloon-borne direct sun DOAS (Differential Optical Absorption Spectroscopy) BrO observations (Dorf et al., 2006; Carpenter et al., 2014) and annual mean mixing ratios derived from ground-based UV-visible measurements of stratospheric BrO (Sinnhuber et al., 2002; Hendrick et al., 2007; Hendrick et al., 2008; Carpenter et al., 2014). These observations show the temporal development of Br_y in dependence of the year when air masses are entering the stratosphere. Assuming a mean age of air of 6 years at 25 km (Haenel et al., 2015) we can compare the measured Br_y from MIPAS-B directly to the Br_y from DOAS observations in the years (of stratospheric entry) 2005 and 2008. In these years, the range of expected Br_y spans from about 18 to 25 pptv taking into account the error limits. Although the amount of Br_y inferred from MIPAS-B measurements lies more towards the upper edge of this range, it is still consistent with the Br_y estimates from DOAS observations.

4 Conclusions

$BrONO_2$ observations around sunrise were performed during balloon flights with MIPAS-B carried out in the Arctic from Kiruna on 24 January 2010 and 31 March 2011 and at mid-latitudes from Timmins on 7/8 September 2014. Measured $BrONO_2$ diurnal variations with high nighttime and low daytime values confirm the stratospheric bromine chemistry (introduced in Sect. 1) that is dominated by the interaction of BrO and $BrONO_2$ according to (R1) – (R3). During polar winter (January 2010) with weak illumination, large parts of nighttime Br_y are in the form of BrCl resulting in significantly lower $BrONO_2$ values compared to the situation in late Arctic winter (March 2011) and mid-latitude summer (September 2014).

The chemistry climate model EMAC is able to reproduce the temporal variation of the measured $BrONO_2$ values. However, some differences in the absolute amounts of $BrONO_2$ are obvious. The simulated $BrONO_2$ mixing ratios are dependent on the assumed total Br_y in the model, which amounts about 23 pptv in the lower stratosphere. As mentioned in Sect. 2.3 reactions of short-lived bromine-containing organic compounds are integrated into the model setup according to emission scenarios shown by Warwick et al. (2006). This is equivalent to about 6-7 pptv inorganic bromine from these oceanic short-lived bromocarbons in the upper troposphere.

As discussed in Sect. 3.3, Br_y in the lower stratosphere was estimated from MIPAS-B measurements. For the Arctic observation in March 2011, we obtain 22.3 ± 2.2 pptv Br_y and for the mid-latitude measurement in September 2014, we calculate 23.6 ± 1.9 pptv Br_y in the lower stratosphere. These values are consistent with the range of Br_y estimates from DOAS observations.

Finally, it should be mentioned that there is still some limited potential on the improvement of the spectroscopy of the interfering species (mainly HO_2NO_2) in the $BrONO_2$ spectral analysis window (Wagner and Birk, 2016). However, $BrONO_2$ test retrieval simulations for MIPAS-B (within this work) and MIPAS (Höpfner et al., 2009) have shown that future improvements in the spectroscopic database will most probably not exceed the total error limits given in this study.

Acknowledgements

We are grateful to the CNES balloon team for excellent balloon operations and the Swedish Space Corporation for operating Arctic campaigns and logistical assistance. We thank Katja Grunow from Free University of Berlin for meteorological support. The work presented here was funded in part by the European Space Agency (ESA) and the German Aerospace Center (DLR). We acknowledge support by Deutsche Forschungsgemeinschaft and Open Access Publishing Fund of Karlsruhe Institute of Technology.

References

Atkinson, R., Baulch, D. L., Cox, R. A., Crowley, J. N., Hampson, R. F., Hynes, R. G., Jenkin, M. E., Rossi, M. J., and Troe, J.: Evaluated kinetic and photochemical data for atmospheric chemistry: Volume III – gas phase reactions of inorganic halogens, Atmos. Chem. Phys., 7, 981-1191, doi:10.5194/acp-7-981-2007, 2007.

Brasseur, G., and Solomon, S.: Aeronomy of the middle atmosphere (third edition), Atmos. Oceanograph. Sci. Lib., p. 369 ff, Springer, Dordrecht, The Netherlands, 2005.

Carpenter, L. J., Reimann, S., Burkholder, J. B., Clerbaux, C., Hall, B. D., Hossaini, R., Laube, J. C., and Yvon-Lewis, S. A.: Ozone-Depleting Substances (ODSs) and other gases of interest to the Montreal Protocol, Chapter 1 in Scientific Assessment of Ozone Depletion: 2014, Global Ozone Research and Monitoring Project – Report No. 55, 416 pp., World Meteorological Organization, Geneva, Switzerland, 2014.

Dee, D. P., Uppala, S. M., Simmons, A. J., Berrisford, P., Poli, P., Kobayashi, S., Andrae, U., Balmaseda, M. A., Balsamo, G., Bauer, P., Bechtold, P., Beljaars, A. C. M., van de Berg, L., Bidlot, J., Bormann, N., Delsol, C., Dragani, R., Fuentes, M., Geer, A. J., Haimberger, L., Healy, S. B., Hersbach, H., Hólm, E. V., Isaksen, L., Kållberg, P., Köhler, M., Matricardi, M., McNally, A. P., Monge-Sanz, B. M., Morcrette, J.-J., Park, B.-K., Peubey, C., deRosnay, P., Tavolato, C., Thépaut, J.-N., F. Vitart, F.: The ERA-Interim reanalysis: configuration and performance of the data assimilation system, Q. J. R. Meteorol. Soc. 137, 553 – 597, 2011.

Dorf, M., Butler, J. H., Butz, A., Camy-Peyret, C., Chipperfield, M. P., Kritten, L., Montzka, S. A., Simmes, B., Weidner, F., and Pfeilsticker, K.: Long-term observations of stratospheric bromine reveal slow down in growth, Geophys. Res. Lett., 33, L24803, doi:10.1029/2006GL027714, 2006.

Flaud, J.-M., Piccolo, C., Carli, B., Perrin, A., Coudert, L.H., Teffo, J.-L., and Brown, L.R.: Molecular line parameters for the MIPAS (Michelson Interferometer for Passive Atmospheric Sounding) experiment, Atmos. Oceanic Opt., 16, 172-182, 2003.

Friedl, R. R., May, R. D., and Duxbury, G.: The ν_6, ν_7, ν_8, and ν_{10} bands of HO_2NO_2, J. Mol. Spectrosc., 165, 481-493, 1994.

Friedl-Vallon, F., Maucher, G., Kleinert, A., Lengel, A., Keim, C., Oelhaf, H., Fischer, H., Seefeldner, M., and Trieschmann, O.: Design and characterization of the balloon-borne

Michelson Interferometer for Passive Atmospheric Sounding (MIPAS-B2), Appl. Opt., 43, 3335-3355, 2004.

Haenel, F. J., Stiller, G. P., von Clarmann, T., Funke, B., Eckert, E., Glatthor, N., Grabowski, U., Kellmann, S., Kiefer, M., Linden, A., and Reddmann, T.: Reassessment of MIPAS age of air trends and variability, Atmos. Chem. Phys., 15, 13161–13176, doi:10.5194/acp-15-13161-2015, 2015.

Hendrick, F., Van Roozendael, M., Chipperfield, M. P., Dorf, M., Goutail, F., Yang, X., Fayt, C., Hermans, C., Pfeilsticker, K., Pommereau, J.-P., Pyle, J. A., Theys, N., and De Mazière, M.: Retrieval of stratospheric and tropospheric BrO profiles and columns using ground-based zenith-sky DOAS observations at Harestua, 60° N, Atmos. Chem. Phys., 7, 4869-4885, doi:10.5194/acp-7-4869-2007, 2007.

Hendrick, F., Johnston, P. V., De Mazière, M., Fayt, C., Hermans, C., Kreher, K., Theys, N., Thomas, A., and Van Roozendael, M.: One-decade trend analysis of stratospheric BrO over Harestua (60°N) and Lauder (45°S) reveals a decline, Geophys. Res. Lett., 35, L14801, doi:10.1029/2008GL034154, 2008.

Höpfner, M., Oelhaf, H., Wetzel, G., Friedl-Vallon, F., Kleinert, A., Lengel, A., Maucher, G., Nordmeyer, H., Glatthor, N., Stiller, G., von Clarmann, T., Fischer, H., Kröger, C., and Deshler, T.: Evidence of scattering of tropospheric radiation by PSCs in mid-IR limb emission spectra: MIPAS-B observations and KOPRA simulations, Geophys. Res. Lett., 29(8), 1278, doi:10.1029/2001GL014443, 2002.

Höpfner, M., Orphal, J., von Clarmann, T., Stiller, G., and Fischer, H.: Stratospheric $BrONO_2$ observed by MIPAS, Atmos. Chem. Phys., 9, 1735–1746, doi:10.5194/acp-9-1735-2009, 2009.

Jöckel, P., Kerkweg, A., Pozzer, A., Sander, R., Tost, H., Riede, H., Baumgaertner, A., Gromov, S., and Kern, B.: Development cycle 2 of the Modular Earth Submodel System (MESSy2), Geosci. Model Dev., 3, 717-752, doi:10.5194/gmd-3-717-2010, 2010.

Jöckel, P., Tost, H., Pozzer, A., Kunze, M., Kirner, O., Brenninkmeijer, C. A. M., Brinkop, S., Cai, D. S., Dyroff, C., Eckstein, J., Frank, F., Garny, H., Gottschaldt, K.-D., Graf, P., Grewe, V., Kerkweg, A., Kern, B., Matthes, S., Mertens, M., Meul, S., Neumaier, M., Nützel, M., Oberländer-Hayn, S., Ruhnke, R., Runde, T., Sander, R., Scharffe, D., and Zahn, A.: Earth System Chemistry integrated Modelling (ESCiMo) with the Modular Earth Submodel

System (MESSy) version 2.51, Geosci. Model Dev., 9, 1153-1200, doi:10.5194/gmd-9-1153-2016, 2016.

Kirner, O., Ruhnke, R., Buchholz-Dietsch, J., Jöckel, P., Brühl., C., and Steil, B.: Simulation of polar stratospheric clouds in the chemistry-climate-model EMAC via the submodel PSC, Geosci. Model Dev., 4, 169-182, doi:10.5194/gmd-4-169-2011, 2011.

Kleinert, A.: Correction of detector nonlinearity for the balloonborne Michelson Interferometer for Passive Atmospheric Sounding, Appl. Opt., 45, 425-431, 2006.

Kreycy, S., Camy-Peyret, C., Chipperfield, M. P., Dorf, M., Feng, W., Hossaini, R., Kritten, L., Werner, B., and Pfeilsticker, K.: Atmospheric test of the $J(BrONO_2)/k_{BrO+NO2}$ ratio: implications for total stratospheric Br_y and bromine-mediated ozone loss, Atmos. Chem. Phys., 13, 6263–6274, doi:10.5194/acp-13-6263-2013, 2013.

May, R. D., and Friedl, R. R.: Integrated band intensities of HO_2NO_2 at 220 K, J. Quant. Spectrosc. Radiat. Transfer, 50, 257-266, 1993.

Montzka, S. A., Butler, J. H., Elkins, J. W., Thompson, T. M., Clarke, A. D. and Lock, L. T.: Present and future trends in the atmospheric burden of ozone-depleting halogens, Nature, 398, 690-694, 1999.

Newman, P. A., Daniel, J. S., Waugh, D. W., and Nash, E. R.: A new formulation of equivalent effective stratospheric chlorine (EESC), Atmos. Chem. Phys., 7, 4537–4552, doi:10.5194/acp-7-4537-2007, 2007.

Norton, H., and Beer, R.: New apodization functions for Fourier spectroscopy, J. Opt. Soc. Am., 66, 259-264 (Errata, J. Opt. Soc. Am., 67, 419, 1977.) 1976.

Phillips, D.: A technique for the numerical solution of certain integral equations of the first kind, J. Assoc. Comput. Math., 9, 84–97, 1962.

Raspollini, P., Carli, B., Carlotti, M., Ceccherini, S., Dehn, A., Dinelli, B. M., Dudhia, A., Flaud, J.-M., López-Puertas, M., Niro, F., Remedios, J. J., Ridolfi, M., Sembhi, H., Sgheri, L., and von Clarmann, T.: Ten years of MIPAS measurements with ESA Level 2 processor V6 – Part 1: Retrieval algorithm and diagnostics of the products, Atmos. Meas. Tech., 6, 2419-2439, doi:10.5194/amt-6-2419-2013, 2013.

Remedios, J. J., Leigh, R. J., Waterfall, A. M., Moore, D. P., Sembhi, H., Parkes, I., Greenhough, J., Chipperfield, M. P., and Hauglustaine, D.: MIPAS reference atmospheres

and comparisons to V4.61/V4.62 MIPAS level 2 geophysical data sets, Atmos. Chem. Phys. Discuss., 7, 9973–10017, doi:10.5194/acpd-7-9973-2007, 2007.

Rodgers, C.: Inverse methods for atmospheric sounding: Theory and practice, World Sci., Hackensack, N. J., 2000.

Roeckner, E., Brokopf, R., Esch, M., Giorgetta, M., Hagemann, S., Koernblueh, L., Manzini, E., Schlese, U., and Schulzweida, U.: Sensitivity of simulated climate to horizontal and vertical resolution in the ECHAM5 atmosphere model, J. Climate, 19, 3771-3791, 2006.

Rothman, L. S., Gordon, I. E., Barbe, A., Benner, D. C., Bernath, P. F., Birk, M., Boudon, V., Brown, L. R., Campargue, A., Champion, J.-P., Chance, K., Coudert, L. H., Dana, V., Devi, V. M., Fally, S., Flaud, J.-M., Gamache, R. R., Goldman, A., Jacquemart, D., Kleiner, I., Lacome, N., Lafferty, W. J., Mandin, J.-Y., Massie, S. T., Mikhailenko, S. N., Miller, C. E., Moazzen-Ahmadi, N., Naumenko, O. V., Nikitin, A. V., Orphal, J., Perevalov, V. I., Perrin, A., Predoi-Cross, A., Rinsland, C. P., Rotger, M., Šimečková, M., Smith, M. A. H., Sung, K., Tashkun, S. A., Tennyson, J., Toth, R. A., Vandaele, A. C., and Vander Auwera, J.: The HITRAN 2008 molecular spectroscopic database, J. Quant. Spectrosc. Radiat. Transfer, 110, 533–572, doi:10.1016/j.jqsrt.2009.02.013, 2009.

Sander, R., Kerkweg, A., Jöckel, P., and Lelieveld, J.: Technical note: The new comprehensive atmospheric chemistry module MECCA, Atmos. Chem. Phys., 5, 445-450, doi:10.5194/acp-5-445-2005, 2005.

Sander, S. P., Friedl, R. R., Barker, J. R., Golden, D. M., Kurylo, M. J., Wine, P. H., Abbatt, J., Burkholder, J. B., Kolb, C. E., Moortgat, G. K., Huie, R. E., and Orkin, V. L.: Chemical kinetics and photochemical data for use in atmospheric studies Evaluation no. 17, JPL Publ. 10-6, Jet Propulsion Laboratory, Pasadena, CA, 2011.

Sinnhuber, B.-M., Arlander, D. W., Bovensmann, H., Burrows, J. P., Chipperfield, M. P., Enell, C. F., Frieß, U., Hendrick, F., Johnston, P. V., Jones, R. L., Kreher, K., Mohamed-Tahrin, N., Müller, R., Pfeilsticker, K., Platt, U., Pommereau, J.-P., Pundt, I., Richter, A., South, A. M., Tørnkvist, K. K., Van Roozendael, M., Wagner, T., and Wittrock, F.: Comparison of measurements and model calculations of stratospheric bromine monoxide, J. Geophys. Res., 107(D19), 4398, doi:10.1029/2001JD000940, 2002.

Sinnhuber, B.-M., Rozanov, A., Sheode, N., Afe, O. T., Richter, A., Sinnhuber, M., Wittrock, F., Burrows, J. P., Stiller, G. P., von Clarmann, T., and Linden, A.: Global observations of

stratospheric bromine monoxide from SCIAMACHY, Geophys. Res. Lett., 32, L20810, doi:10.1029/2005GL023839, 2005.

Sinnhuber, B.-M., Sheode, N., Sinnhuber, M., Chipperfield, M. P., and Feng, W.: The contribution of anthropogenic bromine emissions to past stratospheric ozone trends: a modelling study, Atmos. Chem. Phys., 9, 2863–2871, doi:10.5194/acp-9-2863-2009, 2009.

Sinnhuber, B.-M., and Meul, S.: Simulating the impact of emissions of brominated very short lived substances on past stratospheric ozone trends, Geophys. Res. Lett., 42, 2449-2456, doi:10.1002/2014GL062975, 2015.

Stiller, G. P., von Clarmann, T., Funke, B., Glatthor, N., Hase, F., Höpfner, M., and Linden, A.: Sensitivity of trace gas abundances retrievals from infrared limb emission spectra to simplifying approximations in radiative transfer modeling, J. Quant. Spectrosc. Radiat. Transfer, 72(3), 249-280, 2002.

Stolarski, R. S., Douglass, A. R., Newman, P. A., Pawson, P., and Schoeberl, M. R.: Relative contribution of greenhouse gases and ozone-depleting substances to temperature trends in the stratosphere: A Chemistry-Climate Model study, J. Clim., 23, 28–42, 2010.

Tikhonov, A.: On the solution of incorrectly stated problems and a method of regularization, Dokl. Acad. Nauk SSSR, 151, 501–504, 1963.

van Aalst, M. K.: Dynamics and Transport in the Stratosphere - simulations with a general circulation model, Ph.D. thesis, Institute for Marine and Atmospheric Research Utrecht, The Netherlands, 2005.

Wagner, G., and Birk, M.: New infrared spectroscopic database for chlorine nitrate, J. Quant. Spectrosc. Radiat. Transfer, 82, 443-460, 2003.

Wagner, G., and Birk, M.: New infrared spectroscopic database for bromine nitrate, J. Mol. Spectrosc., 326, 95-105, 2016.

Warwick, N. J., Pyle, J. A., Carver, G. D., Yang, X., Savage, N. H., O'Connor, F. M., and Cox, R. A.: Global modeling of biogenic bromocarbons, J. Geophys. Res., 111, D24305, doi:10.1029/2006JD007264, 2006.

Wetzel, G., Oelhaf, H., Kirner, O., Friedl-Vallon, F., Ruhnke, R., Ebersoldt, A., Kleinert, A., Maucher, G., Nordmeyer, H., and Orphal, J.: Diurnal variations of reactive chlorine and

nitrogen oxides observed by MIPAS-B inside the January 2010 Arctic vortex, Atmos. Chem. Phys., 12, 6581-6592, doi:10.5194/acp-12-6581-2012, 2012.

Wetzel, G., Oelhaf, H., Birk, M., de Lange, A., Engel, A., Friedl-Vallon, F., Kirner, O., Kleinert, A., Maucher, G., Nordmeyer, H., Orphal, J., Ruhnke, R., Sinnhuber, B.-M., and Vogt, P.: Partitioning and budget of inorganic and organic chlorine species observed by MIPAS-B and TELIS in the Arctic in March 2011, Atmos. Chem. Phys., 15, 8065-8076, doi:10.5194/acp-15-8065-2015, 2015.

Table 1. Overview of MIPAS balloon flights and number of limb sequences recorded around sunrise (Kiruna) and sunset (Timmins). Measurement times are given in UTC and local solar time (LST) together with the solar zenith angle (SZA). Latitude and Longitude refer to the tangent points of the observations.

Location	Date	UTC	LST	SZA (deg)	# Seq.	Latitude (°N)	Longitude (°E)
Kiruna	24 Jan 2010	06:17 – 10:21	08:13 – 12:36	98.1 – 86.2	19	69.3 – 66.9	28.8 – 33.7
Kiruna	31 Mar 2011	02:00 – 04:38	04:01 – 06:34	99.4 – 83.1	12	64.0 – 63.5	30.1 – 28.9
Timmins	7/8 Sep 2014	21:40 – 02:33	16:25 – 21:00	69.9 – 115.1	37	45.9 – 46.2	-78.8 – -83.2

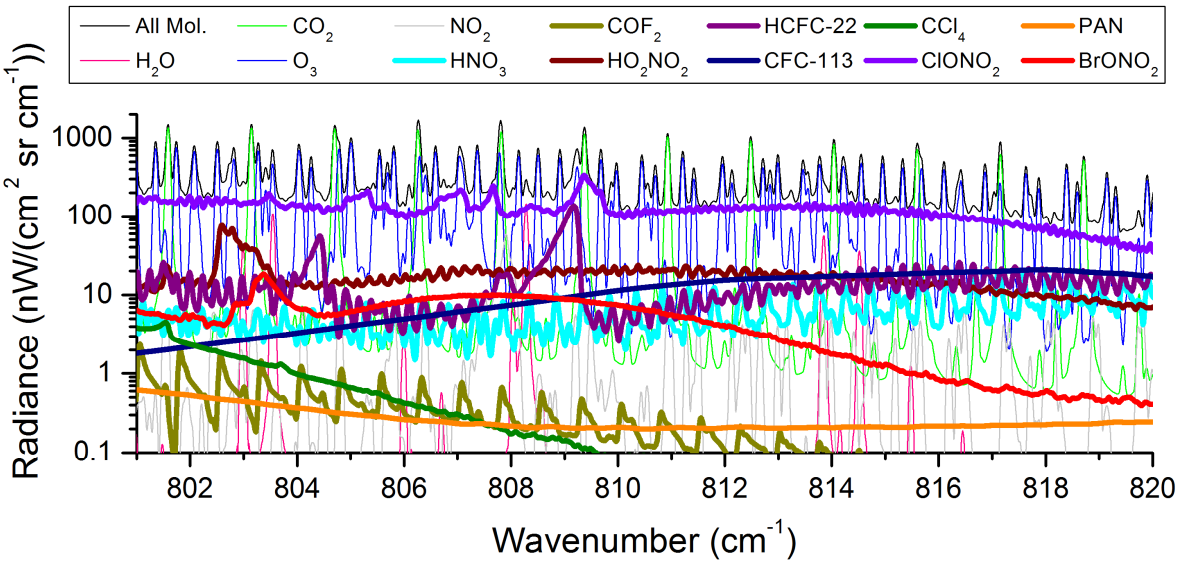

Figure 1. Simulated limb emission spectra (with spectral resolution of MIPAS-B) for a mid-latitude summer standard atmosphere (Remedios et al., 2007) in the spectral region of the $BrONO_2$ analysis window for a tangent altitude of 20 km. Emissions of individual species contributing to the combined spectrum (all molecules, black line) are shown.

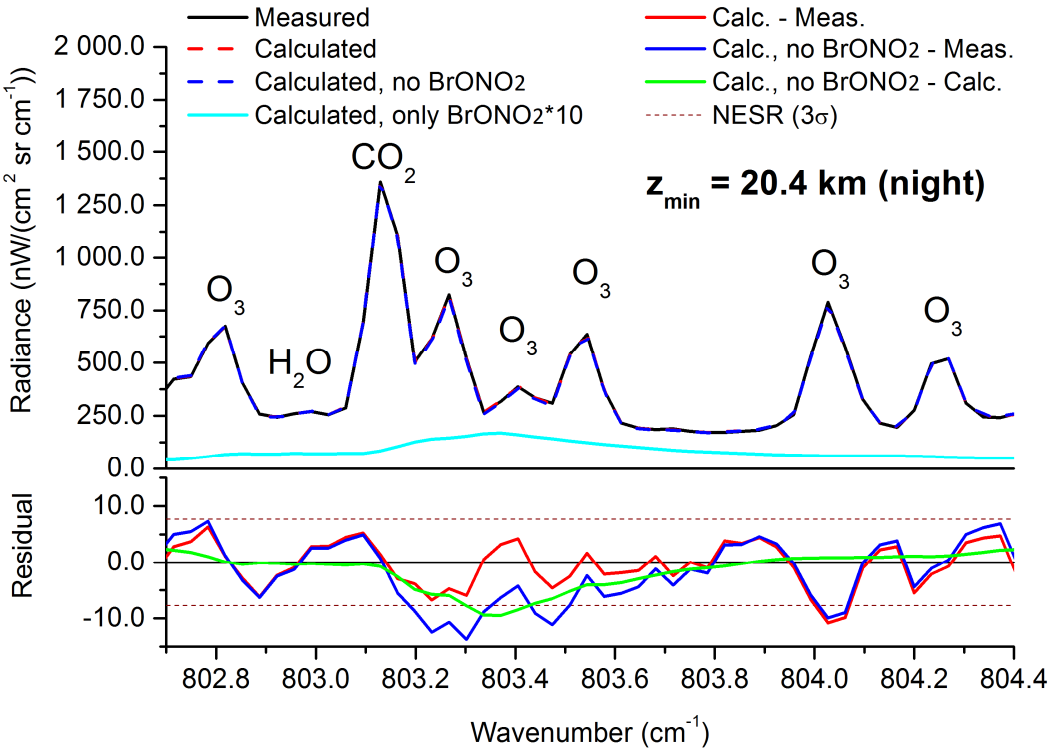

Figure 2. Top panel: Best fit of measured spectrum (black solid line) zoomed around the Q-branch of the $BrONO_2$ ν_3 fundamental band at 803.37 cm^{-1} for a tangent altitude (z_{min}) near 20 km recorded during night on 7/8 September 2014 above Timmins (Seq. 05a). A calculation with (red dashed line) and without (blue dashed line) $BrONO_2$ in the model atmosphere was performed. The calculated individual emission of the $BrONO_2$ band (scaled by a factor of 10; cyan solid line) is shown, too. Bottom panel: Difference between the calculated and measured spectrum (red solid line); difference between the calculated spectrum (without $BrONO_2$) and the measured one (blue solid line); difference of both calculations (green solid line). The 3-σ NESR (brown dotted line) is displayed, too.

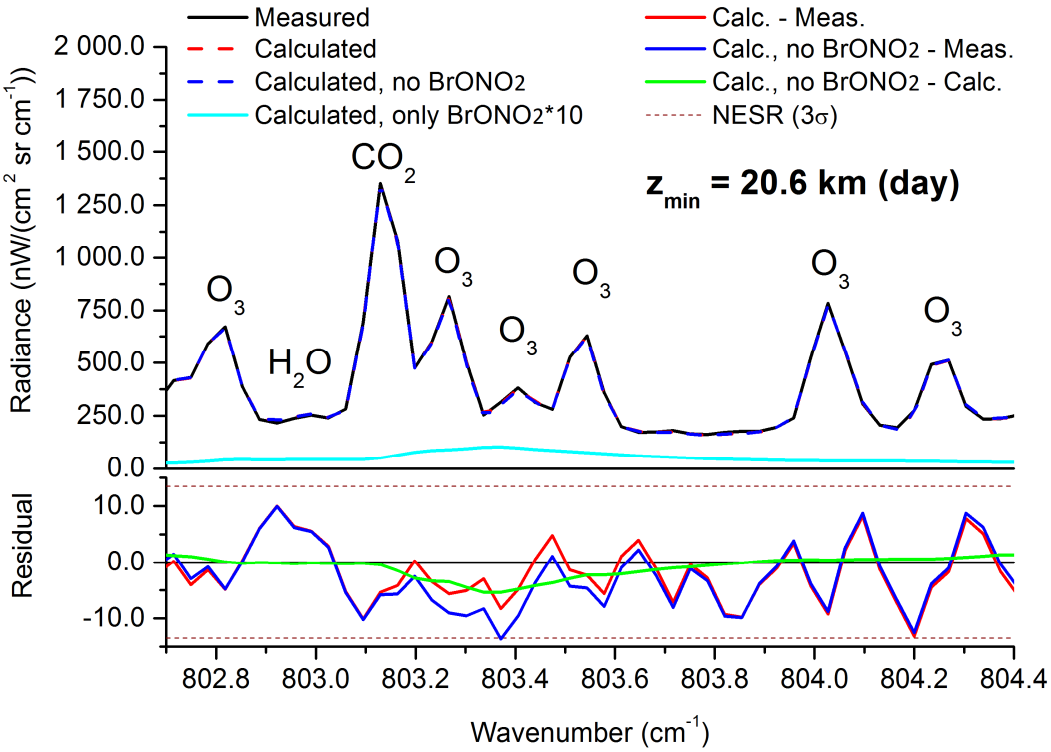

Figure 3. Same as Figure 2 but for a spectrum observed during day (Seq. 02e). The difference between the red and blue solid line (bottom panel) is smaller than the corresponding nighttime difference shown in Figure 2. Hence, $BrONO_2$ amounts seen during day are lower than the ones observed at night.

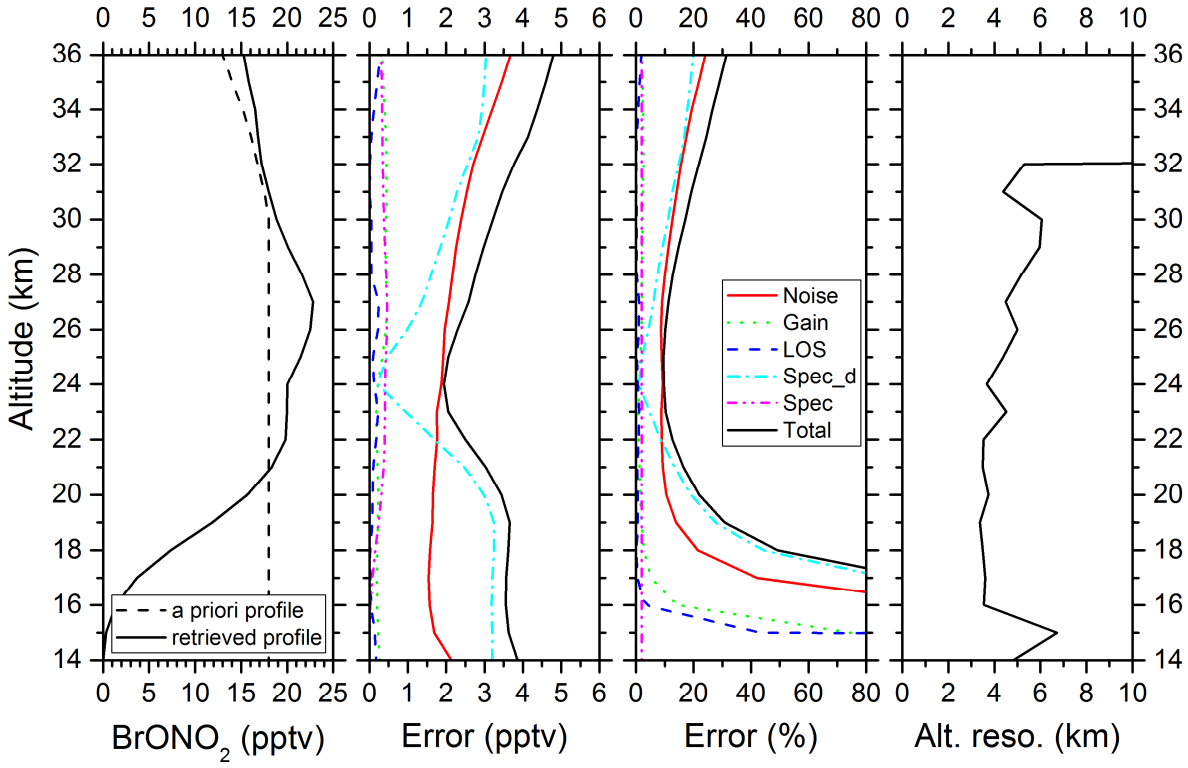

Figure 4. Retrieved $BrONO_2$ VMR vertical profile (and a priori profile) for a nighttime (Seq. 05a) limb sequence recorded by MIPAS-B on 7/8 September 2014 above Timmins together with absolute and relative errors and the altitude resolution, determined from the full width at half maximum of the columns of the averaging kernel matrix. The following error contributions are shown: spectral noise (red solid line), radiometric gain (green dotted line), LOS (blue dashed line), spectroscopic data of disturbing gases (dash dotted cyan line), spectroscopic data of target molecule $BrONO_2$ (short dash dotted magenta line), and total error (black solid line).

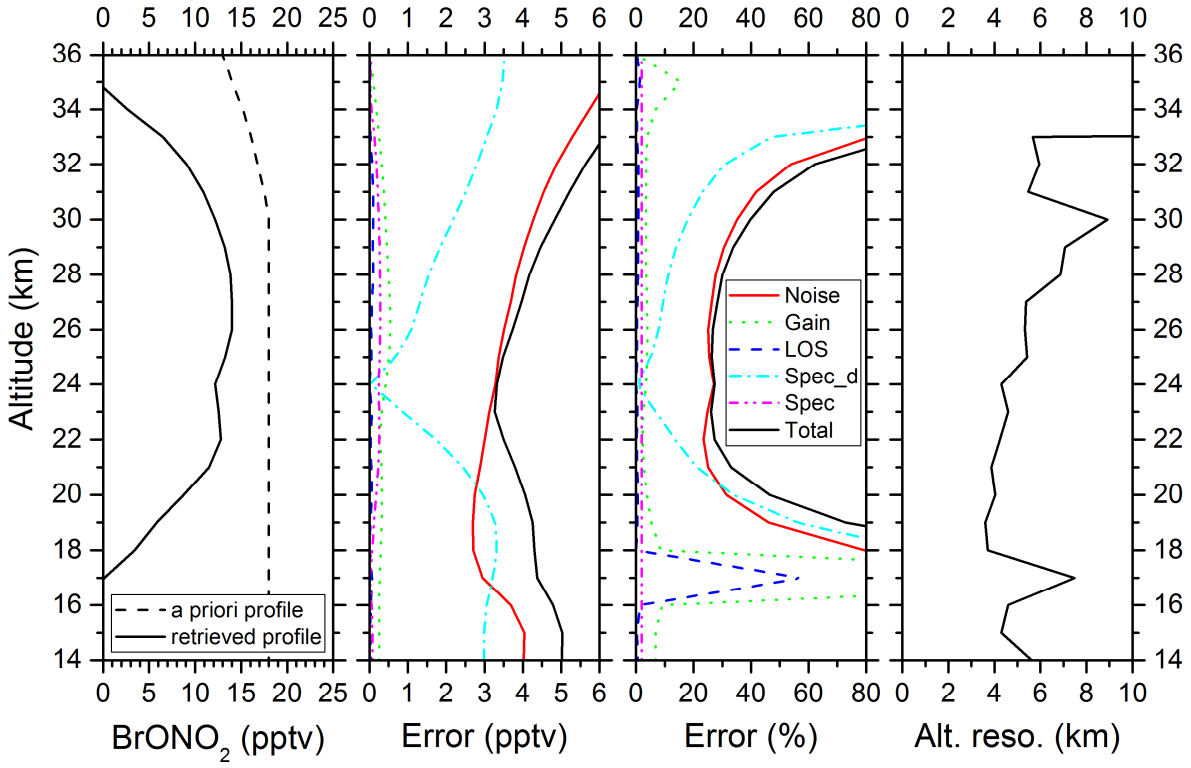

Figure 5. Same as Figure 4 but for a limb sequence measured during day (Seq. 02e).

530

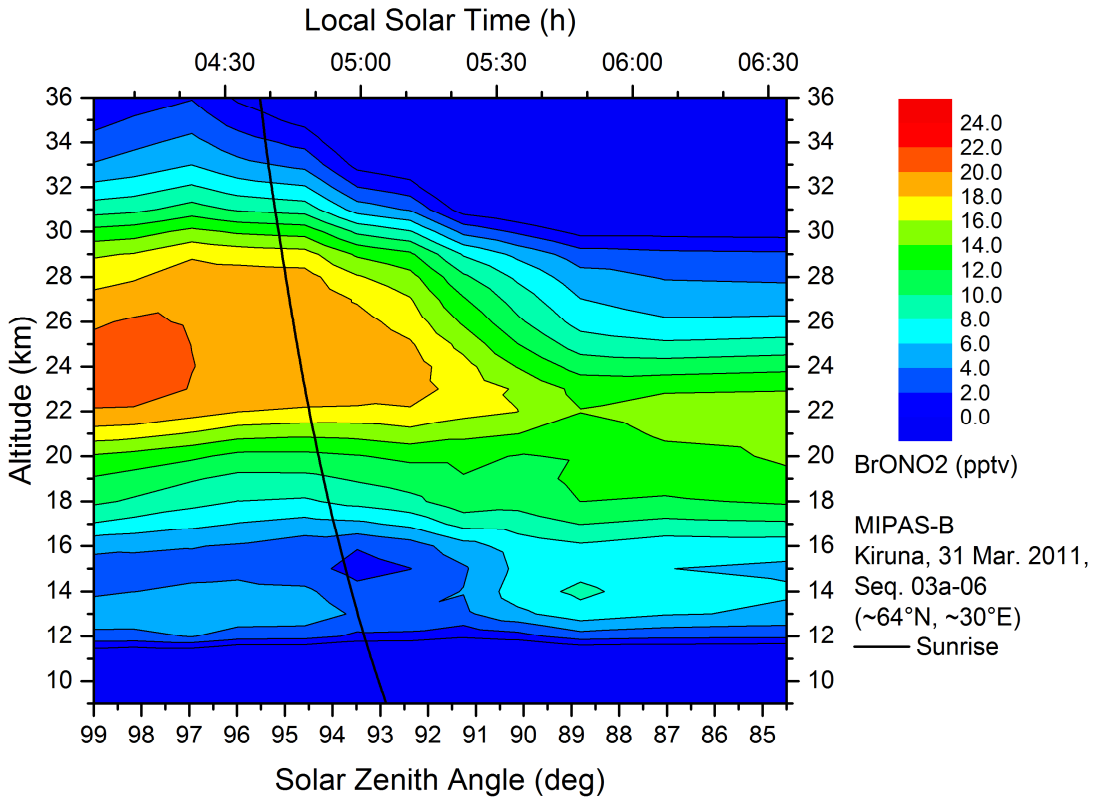

Figure 6. Temporal evolution of $BrONO_2$ volume mixing ratios (pptv) as seen by MIPAS-B from a float altitude around 35 km above northern Scandinavia on 31 March 2011 inside the late winter Arctic vortex. The black solid line marks the sunrise terminator. A decrease in the $BrONO_2$ amount starting around sunrise is clearly visible.

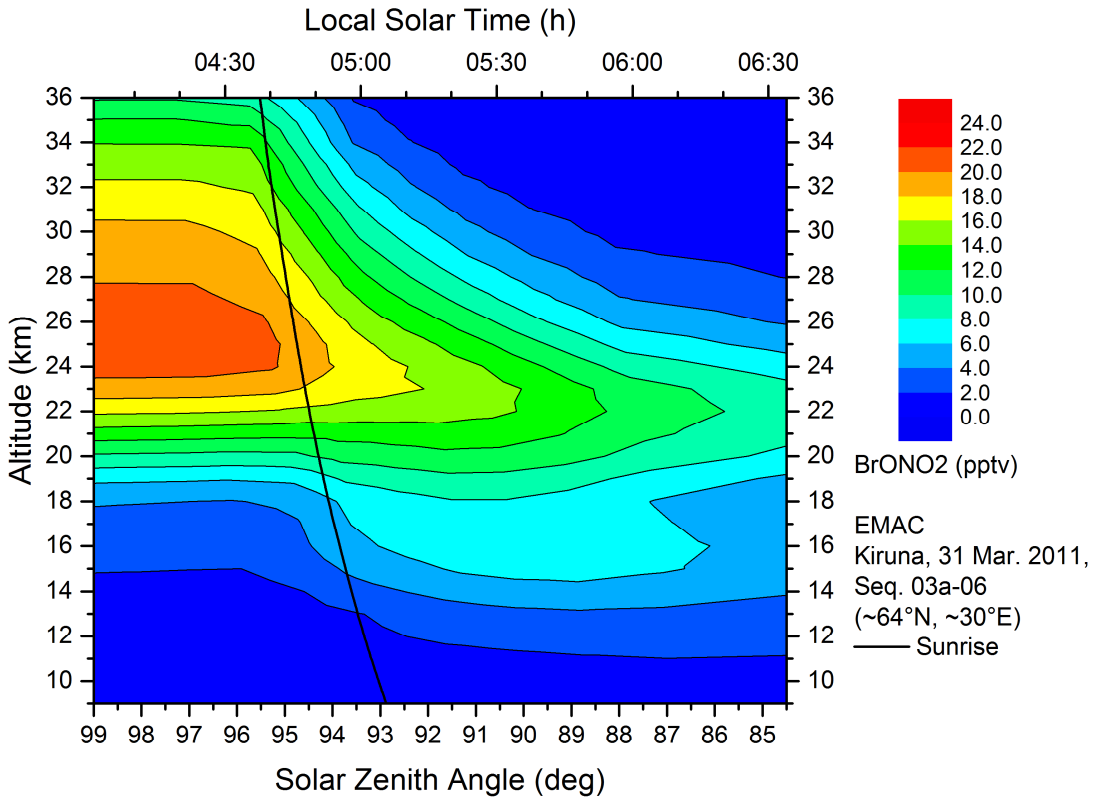

Figure 7. Temporal evolution of $BrONO_2$ on 31 March 2011 as simulated by the chemistry climate model EMAC. The decrease of $BrONO_2$ starts close to sunrise.

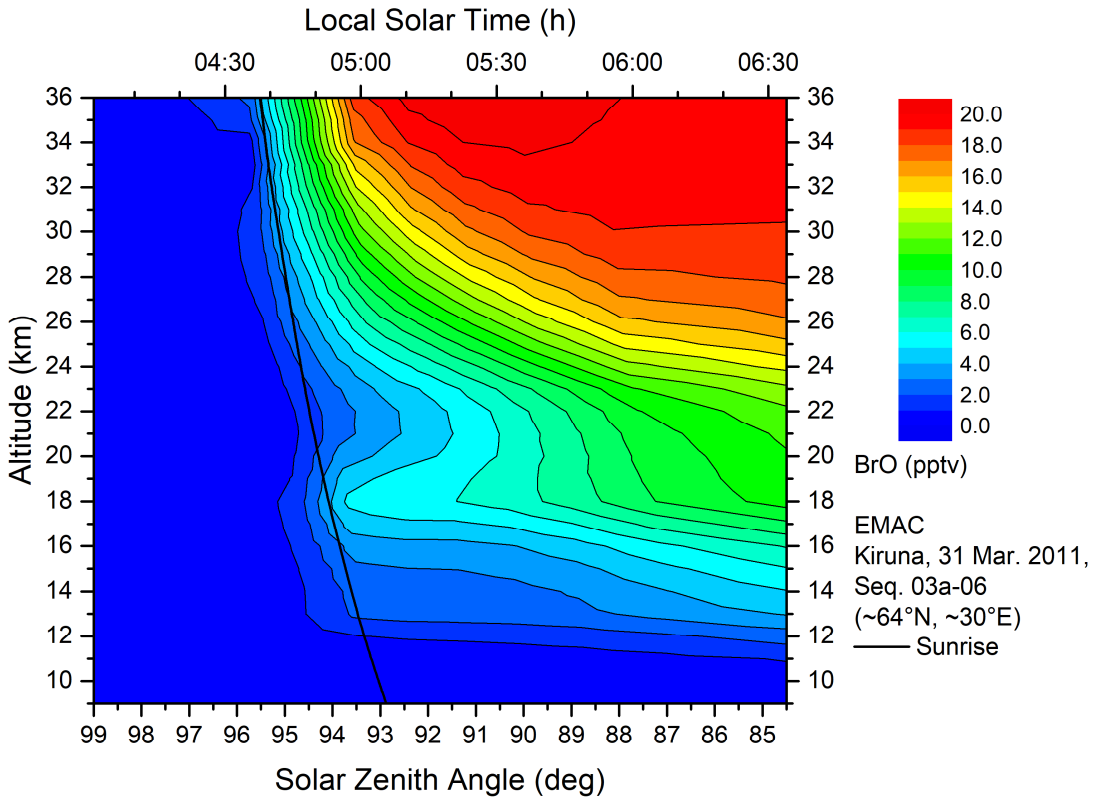

Figure 8. Temporal evolution of BrO on 31 March 2011 as simulated by the chemistry climate model EMAC. The opposite variation with $BrONO_2$ according to (R1) – (R3) is clearly visible.

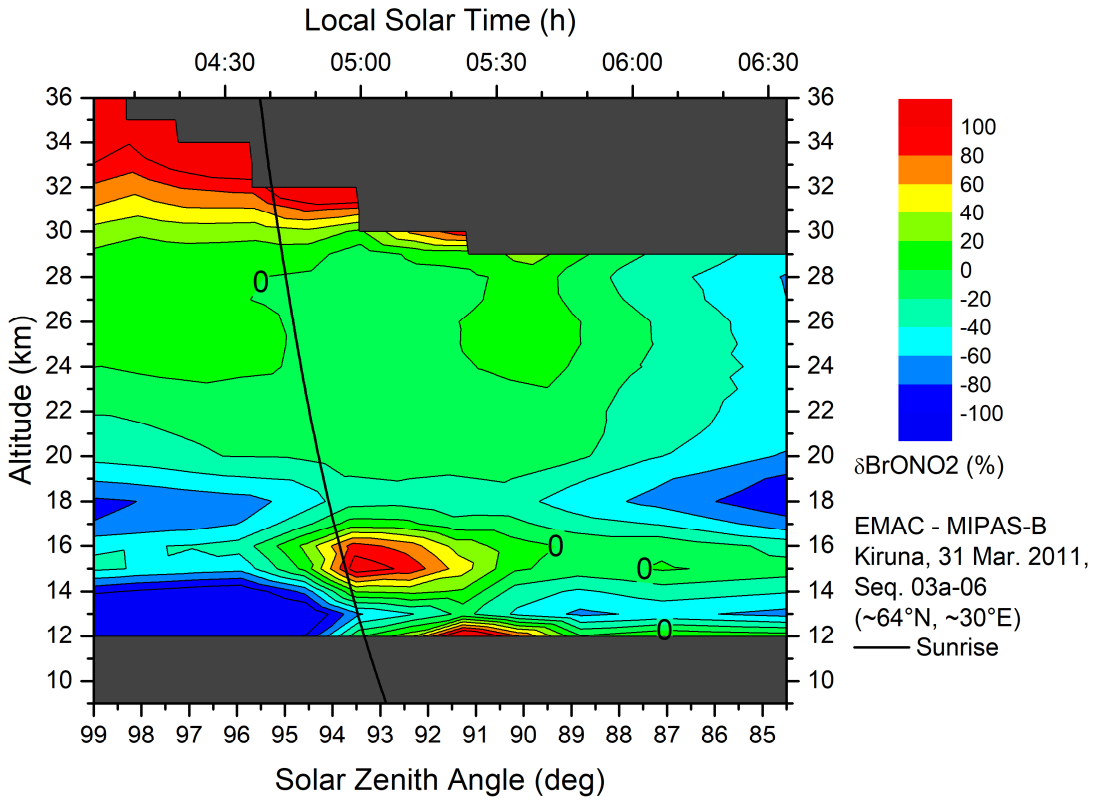

Figure 9. Relative $BrONO_2$ difference between EMAC and MIPAS-B in percent on 31 March 2011. Dark grey regions indicate MIPAS-B values less than zero.

535

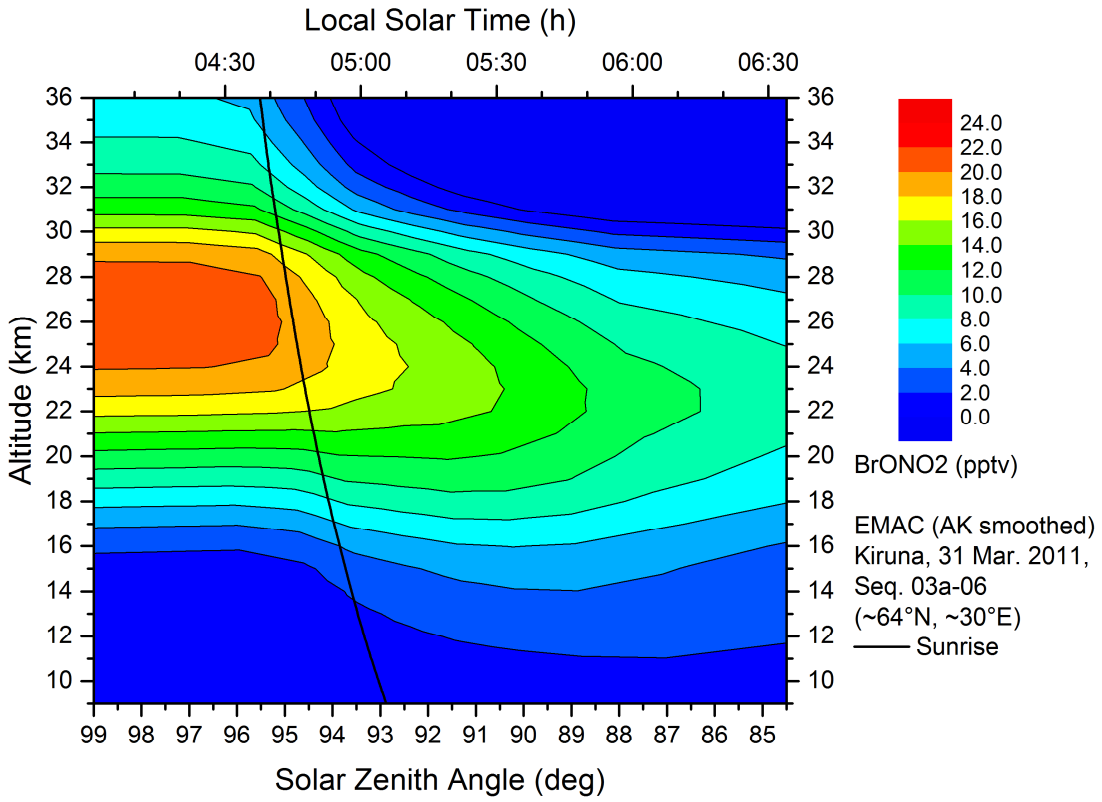

Figure 10. Same as Figure 7 but EMAC vertical profiles smoothed with the MIPAS-B averaging kernel (AK).

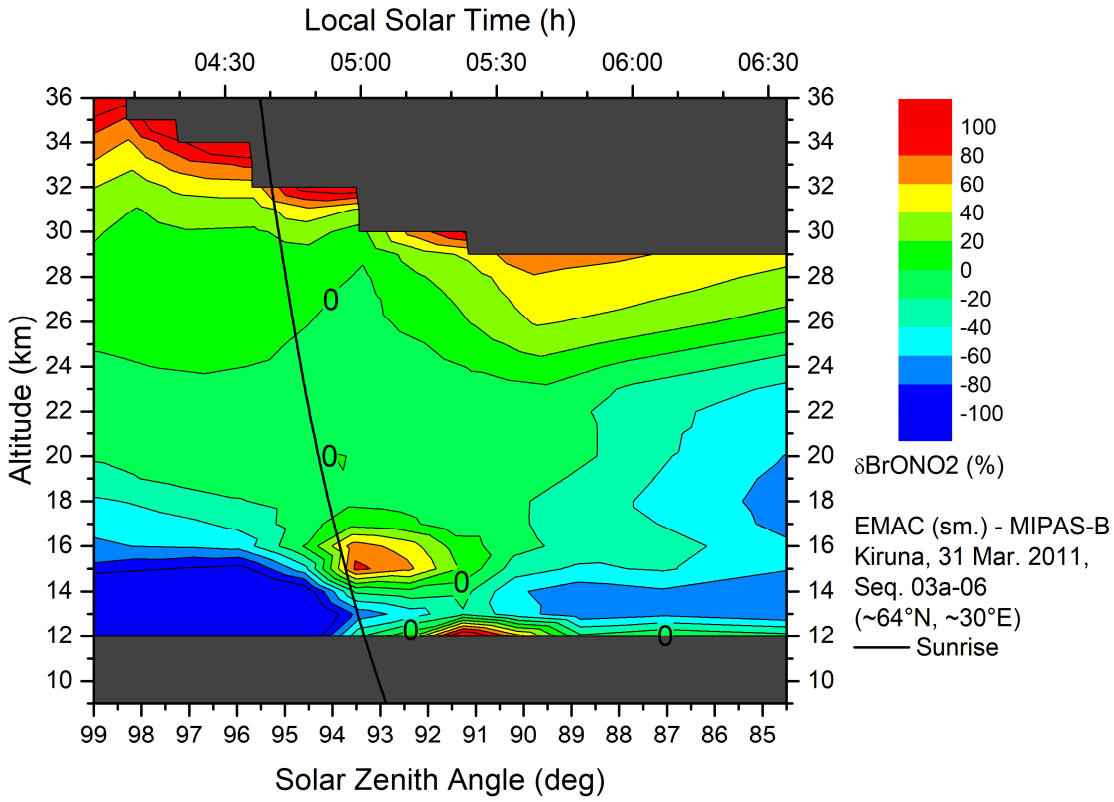

Figure 11. Relative $BrONO_2$ difference between EMAC (AK smoothed) and MIPAS-B in percent on 31 March 2011. Dark grey regions indicate MIPAS-B values less than zero.

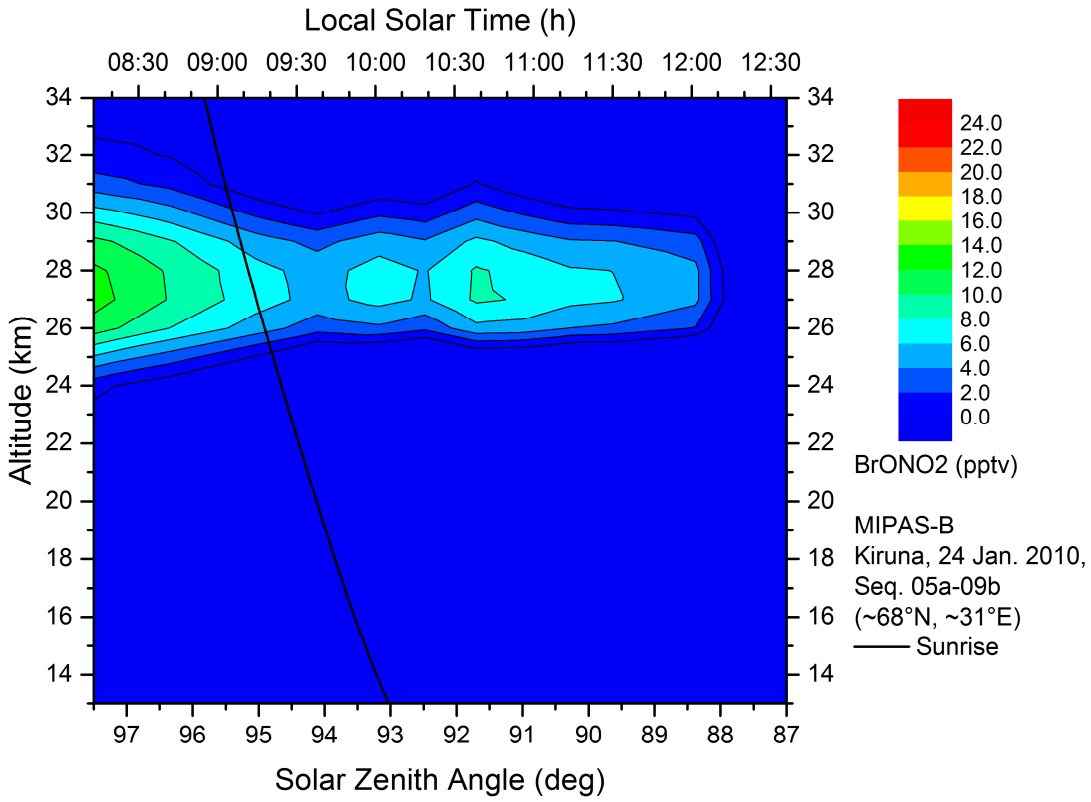

Figure 12. Temporal evolution of $BrONO_2$ volume mixing ratios (pptv) as measured by MIPAS-B on 24 January 2010 inside the mid-winter Arctic vortex (observer altitude about 34 km). The black solid line marks the sunrise terminator. The still weak illumination at the end of the polar night is responsible for the small diurnal variation of the $BrONO_2$ amount.

540

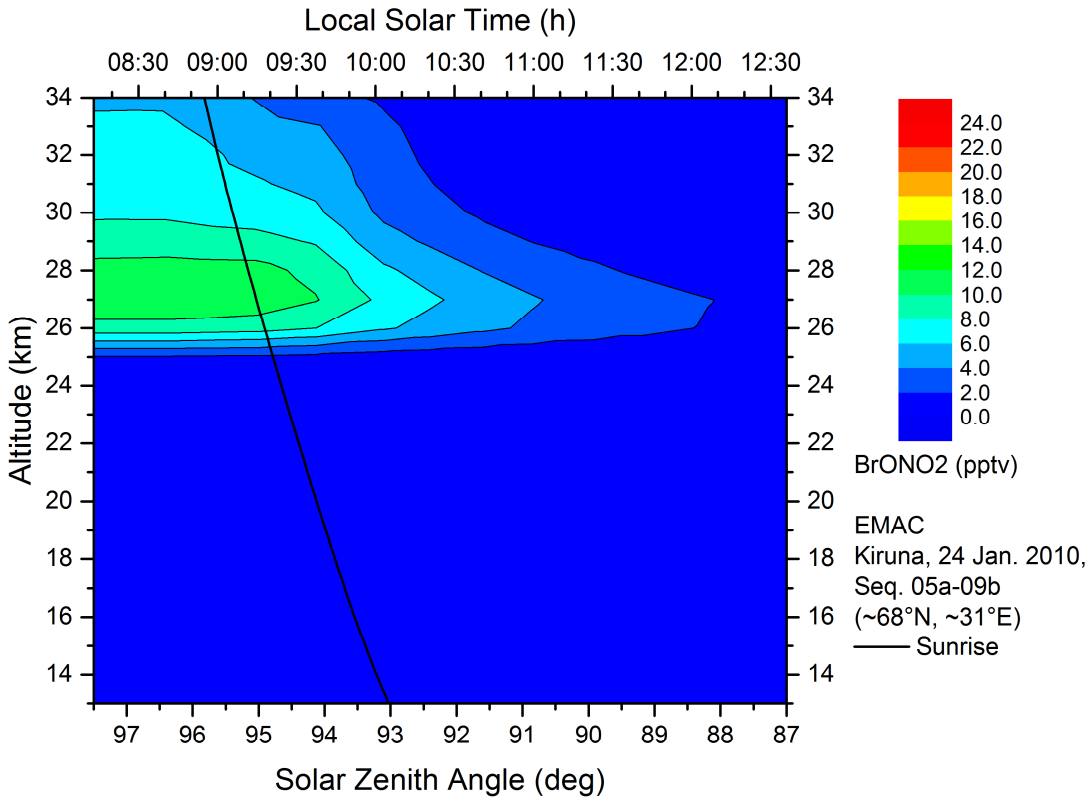

Figure 13. Temporal evolution of $BrONO_2$ on 24 January 2010 as simulated by the chemistry climate model EMAC. The decrease of $BrONO_2$ starts close to sunrise.

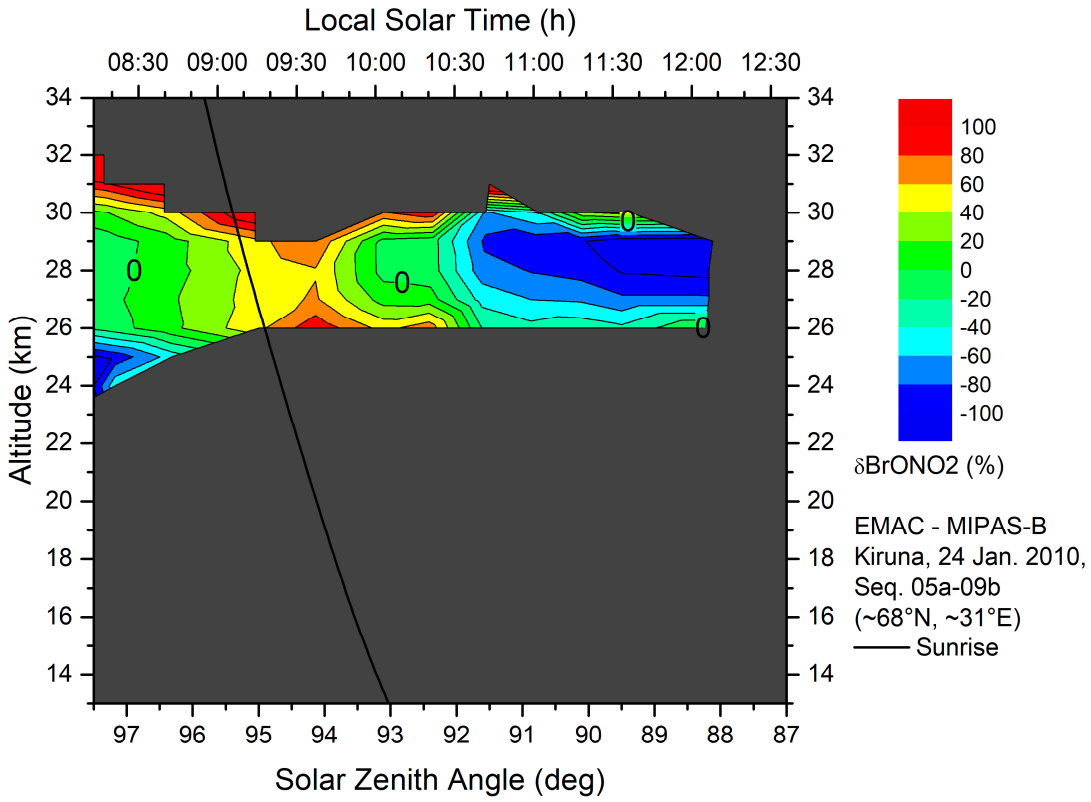

Figure 14. Relative $BrONO_2$ difference between EMAC and MIPAS-B in percent on 24 January 2010. Dark grey regions indicate MIPAS-B values less than zero.

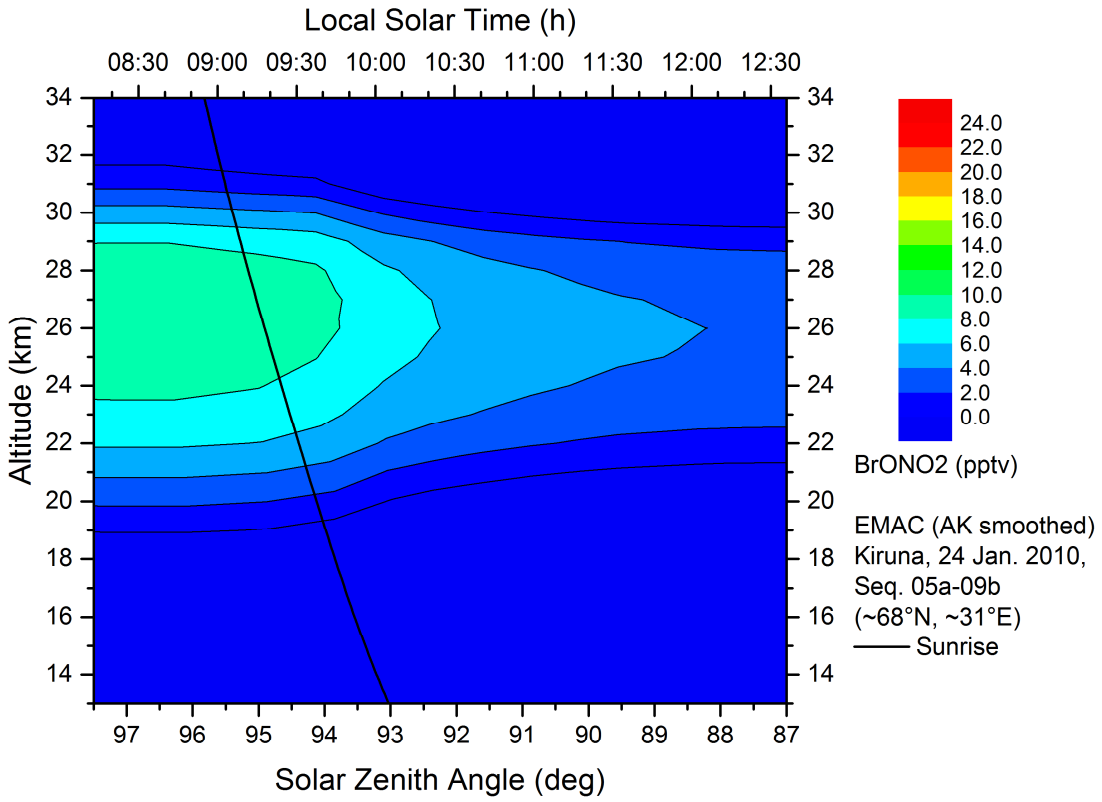

Figure 15. Same as Figure 13 but EMAC vertical profiles smoothed with the MIPAS-B averaging kernel (AK).

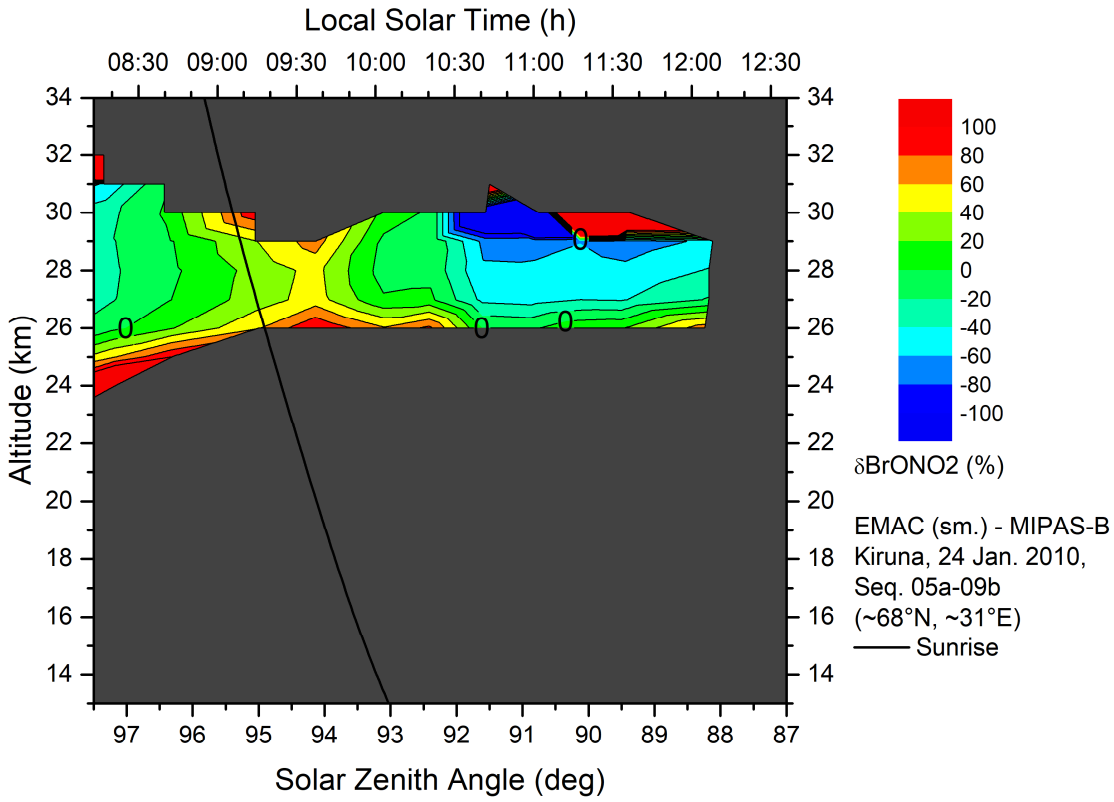

Figure 16. Relative $BrONO_2$ difference between EMAC (AK smoothed) and MIPAS-B in percent on 24 January 2010. Dark grey regions indicate MIPAS-B values less than zero.

545

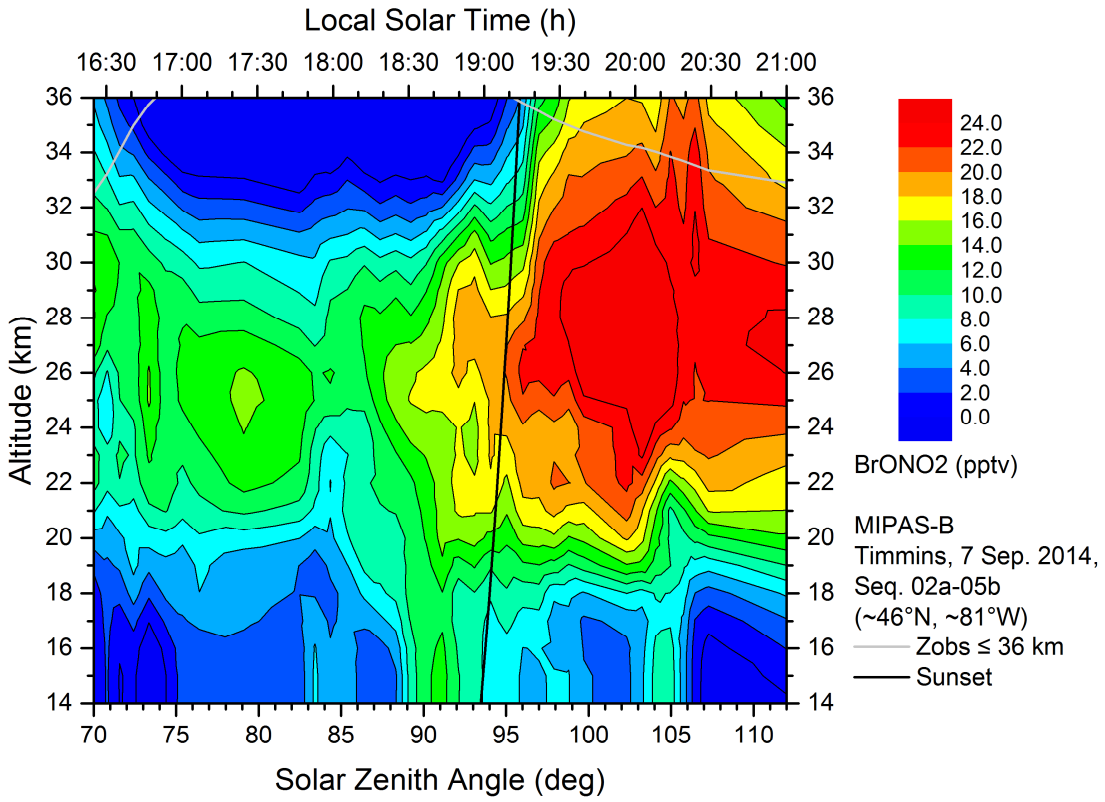

Figure 17. Temporal evolution of $BrONO_2$ amounts observed by MIPAS-B near 46°N above Ontario (Canada) on 7 September 2014. The grey line indicates the time periods where the balloon gondola float altitude was lower or equal to 36 km. The black solid line marks the sunset terminator. The build-up of $BrONO_2$ from daytime BrO starts shortly before sunset.

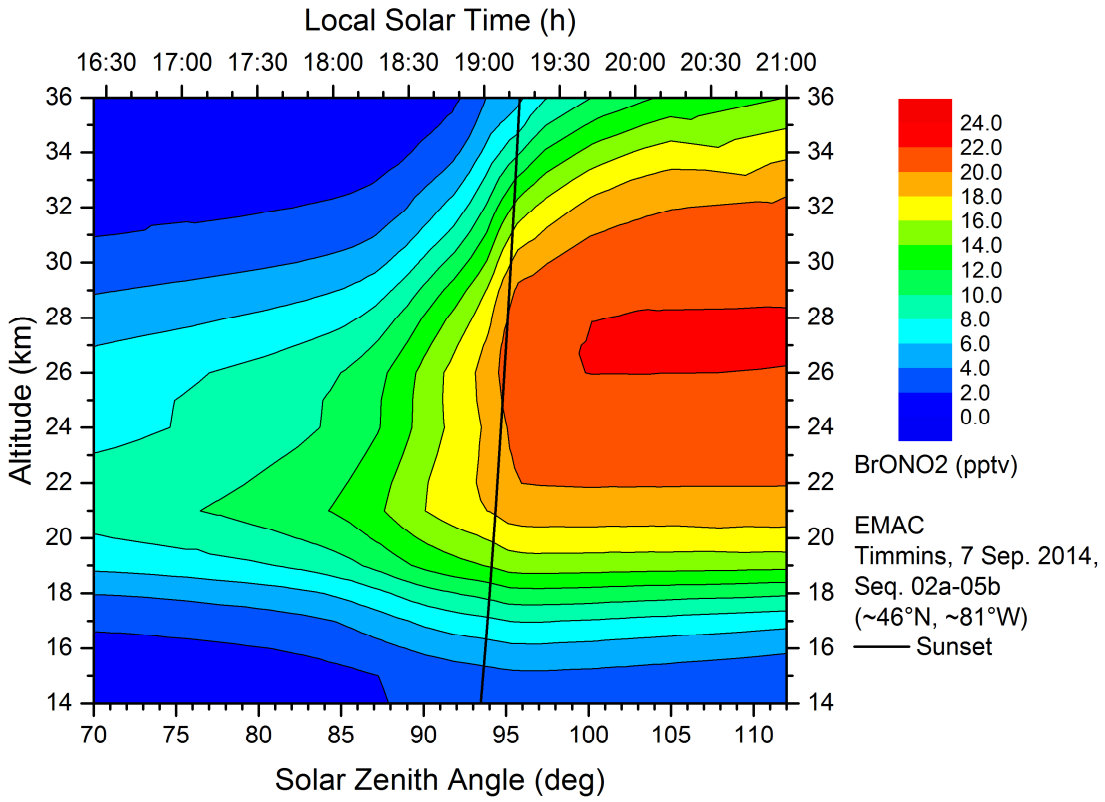

Figure 18. Temporal evolution of $BrONO_2$ on 7 September 2014 as simulated by the EMAC model.

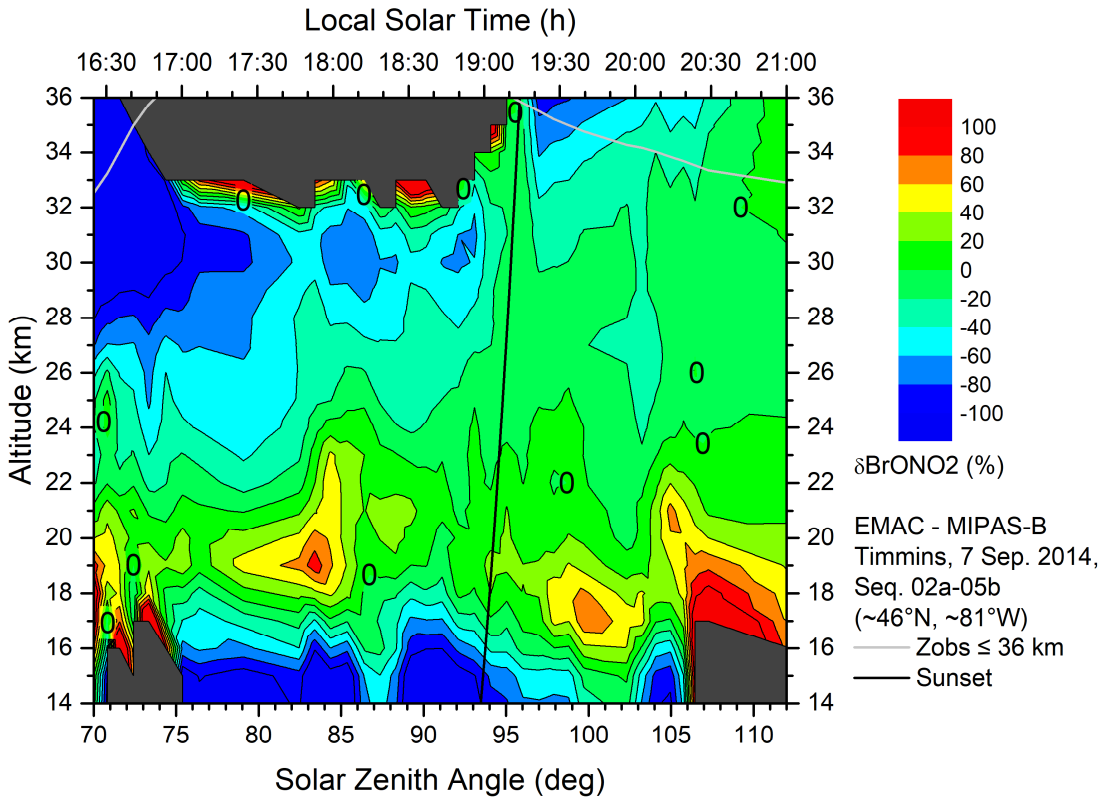

Figure 19. Relative $BrONO_2$ difference between EMAC and MIPAS-B in percent on 7 September 2014. Dark grey regions indicate MIPAS-B values less than zero.

550

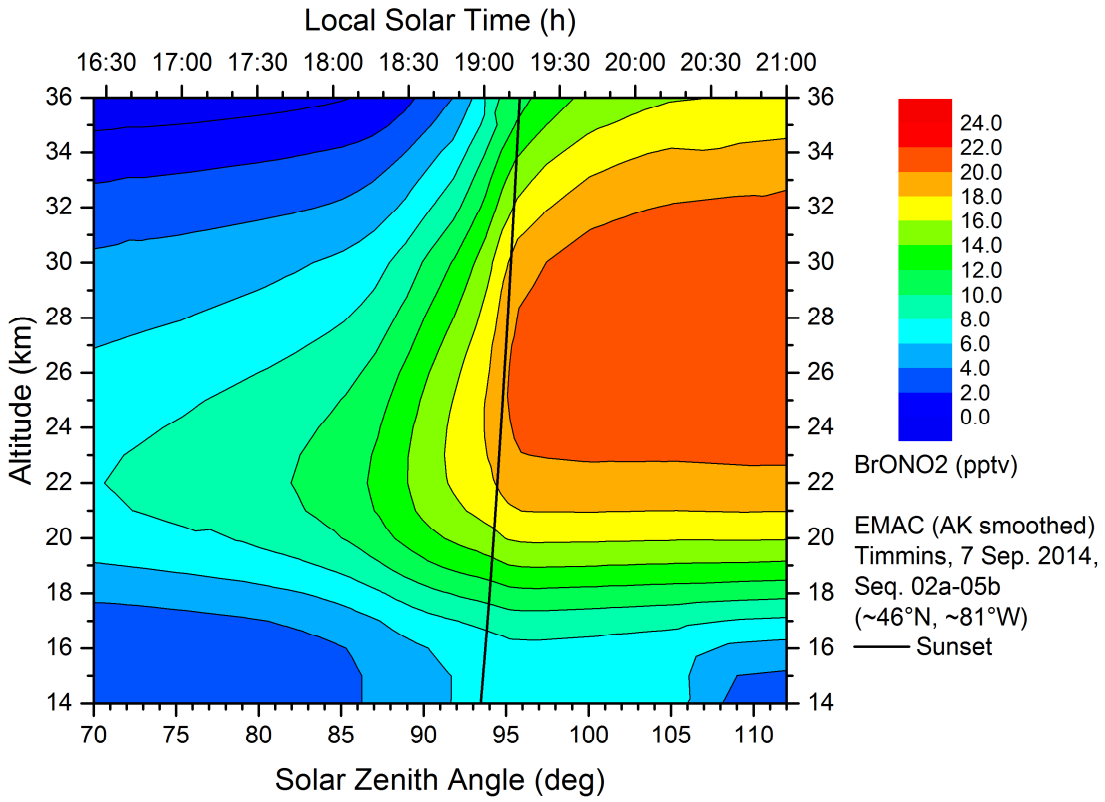

Figure 20. Same as Figure 18 but EMAC vertical profiles smoothed with the MIPAS-B averaging kernel (AK).

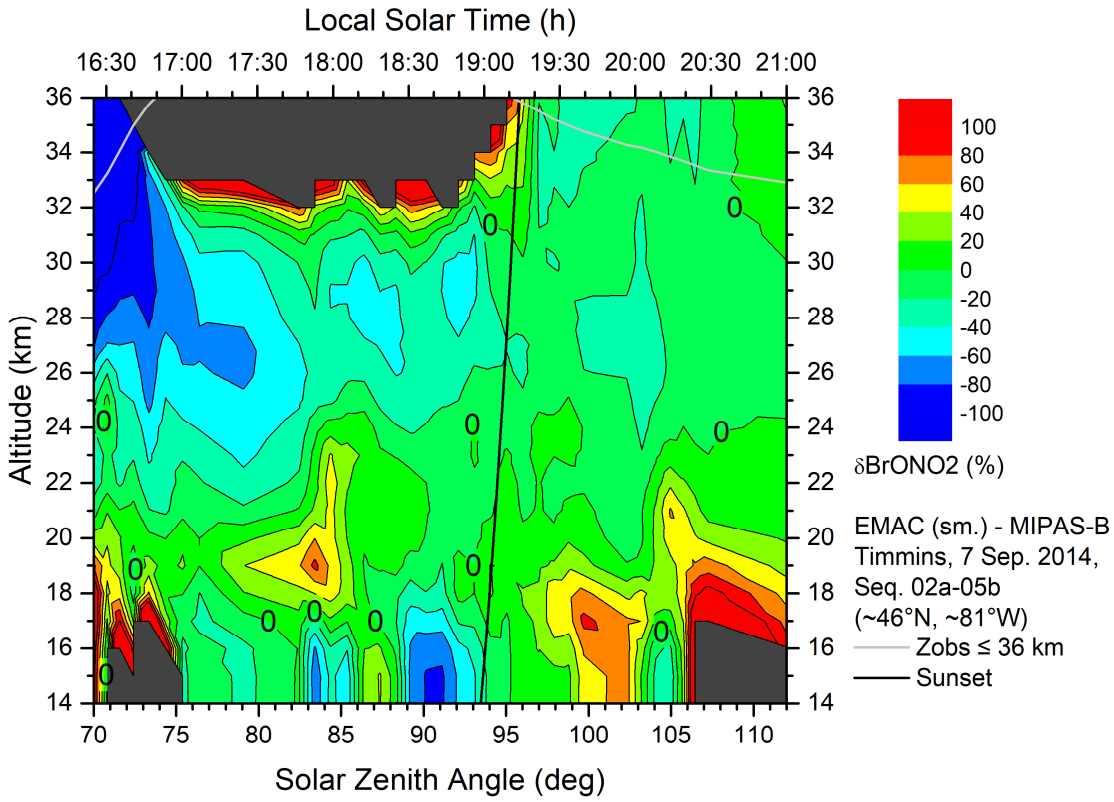

Figure 21. Relative $BrONO_2$ difference between EMAC (AK smoothed) and MIPAS-B in percent on 7 September 2014. Dark grey regions indicate MIPAS-B values less than zero.